Journal of Hydrology: Regional Studies 3 (2015) 285–311

Contents lists available at ScienceDirect

Journal of Hydrology: Regional Studies

journal homepage: www.elsevier.com/locate/ejrh

Assessing the impacts of climate and land use and land cover change on the freshwater availability in the Brahmaputra River basin☆

Md Shahriar Pervez[a,b,*], Geoffrey M. Henebry[b]

[a] ASRC Federal InuTeq, Contractor to U.S. Geological Survey (USGS), Earth Resources Observation and Science (EROS) Center, 47914 252nd Street, Sioux Falls, SD 57198, USA
[b] Geospatial Sciences Center of Excellence (GSCE), South Dakota State University, 1021 Medary Ave., Wecota Hall 506B, Brookings, SD 57007-3510, USA

ARTICLE INFO

Article history:
Received 2 June 2014
Received in revised form 10 September 2014
Accepted 23 September 2014
Available online 25 October 2014

Keywords:
Brahmaputra
Freshwater availability
SWAT
Streamflow
Climate change
Land use change

ABSTRACT

Study Region: Brahmaputra River basin in South Asia.

Study Focus: The Soil and Water Assessment Tool was used to evaluate sensitivities and patterns in freshwater availability due to projected climate and land use changes in the Brahmaputra basin. The daily observed discharge at Bahadurabad station in Bangladesh was used to calibrate and validate the model and analyze uncertainties with a sequential uncertainty fitting algorithm. The sensitivities and impacts of projected climate and land use changes on basin hydrological components were simulated for the A1B and A2 scenarios and analyzed relative to a baseline scenario of 1988–2004.

New hydrological insights for the region: Basin average annual ET was found to be sensitive to changes in CO_2 concentration and temperature, while total water yield, streamflow, and groundwater recharge were sensitive to changes in precipitation. The basin hydrological components were predicted to increase with seasonal variability in response to climate and land use change scenarios. Strong increasing trends were predicted for total water yield, streamflow, and groundwater recharge, indicating exacerbation of flooding potential during August–October, but strong decreasing trends were predicted, indicating exacerbation of drought potential during May–July of the 21st century. The model has potential

☆ Work Performed Under USGS Contract G13PC00028.

* Corresponding author at: ASRC Federal InuTeq, Contractor to U.S. Geological Survey, Earth Resources Observation and Science (EROS) Center, 47914 252nd Street, Sioux Falls, SD 57198, USA. Tel.: +1 605 594 6838; fax: +1 605 594 6529.
E-mail address: spervez@usgs.gov (M.S. Pervez).

http://dx.doi.org/10.1016/j.ejrh.2014.09.003

to facilitate strategic decision making through scenario generation integrating climate change adaptation and hazard mitigation policies to ensure optimized allocation of water resources under a variable and changing climate.

1. Introduction

Climate change is predicted to lead to an intensification of the global hydrological cycle (Huntington, 2006). Freshwater resources in dry subtropical regions may be impacted adversely, but favorably affected at higher latitudes (Cisneros et al., 2014). Quantifying current and future freshwater availability is a critical aspect of adapting to changing and variable climate because access to sufficient freshwater is linked to food security, human health, ecosystem health, land use change, economic development, and regional conflicts (Schuol et al., 2008).

The Brahmaputra River basin located in south Asia is one of the world's major river basins for human and ecological needs and supports the livelihoods of over 66 million people through subsistence agriculture. Despite the growing attention to quantify freshwater resources and to assess the vulnerability of freshwater to global change (Alcamo and Henrichs, 2002; Faramarzi et al., 2009; Lehner et al., 2006; Oki and Kanae, 2006; Piao et al., 2010; Schuol et al., 2008; Srinivasan et al., 1998a,b; Vörösmarty et al., 2000), basinwide assessments of the impacts of climate and land use change on freshwater availability in the Brahmaputra basin remains quite limited.

Increasing concentrations of CO_2 and other greenhouse gases from anthropogenic activities have caused warming of the global climate by modifying radiative forcings (Houghton et al., 2001). Because of the coupling between water and energy balance, any changes in climate will affect the hydrological cycle and the spatial and temporal distribution and intensity of precipitation (Immerzeel, 2008; Labat et al., 2004). The primary source of precipitation in the Brahmaputra basin is the Indian summer monsoon, which is projected to be impacted by global warming (Kripalani et al., 2007; Sabade et al., 2011). Average monsoon precipitation is projected to increase with a possible extension of the monsoon period (Kripalani et al., 2007). Such intensification has been demonstrated to increase the severity of droughts in some parts of India but enhance the intensity of floods in other parts of the country (Gosain et al., 2006). The Indian summer monsoon is linked to a complex set of natural phenomena, including the El Niño–Southern Oscillation (ENSO), Indian Ocean Dipole (IOD) (Ashok et al., 2004; Ashok and Saji, 2007), and Eurasian snow depth levels (Immerzeel, 2008). However, the projected influence of ENSO and IOD on the Indian monsoon is unclear (Cai et al., 2013; Immerzeel, 2008; Jourdain et al., 2013).

Numerous studies have assessed climate change impacts on a particular component of the climatic and hydrological processes in the Brahmaputra basin, e.g. temperature (Immerzeel, 2008; Shi et al., 2011), precipitation (Kripalani et al., 2007), snow (Shi et al., 2011), streamflow (Gain et al., 2011; Jian et al., 2009), groundwater (Tiwari et al., 2009), runoff (Ghosh and Dutta, 2012; Mirza, 2002), extreme events (Rajeevan et al., 2008; Webster and Jian, 2011), and even water quality (Huang et al., 2011). However, few studies have assessed how projected changes in climate and land use and land cover could impact long-term patterns in the basin's hydrological components. Using results from multiple global climate model experiments, Mirza (2002) predicted an increase in the average peak discharge in the Brahmaputra basin. Immerzeel (2008) found that the temperature gradient in the Himalayas (from floodplain to Tibetan Plateau) would likely decrease, resulting in an increase in average precipitation and average seasonal downstream streamflow in the Brahmaputra basin. However, the seasonal streamflow in late spring and summer was eventually predicted to be reduced considerably after a period of increased flows from accelerated glacial melt (Immerzeel et al., 2010). Using results from high-resolution regional climate model experiments, Shi et al. (2011) predicted a 0.57–0.67 °C per decade increase in temperature across the basin and >25% increase in precipitation in the central part of the basin, while increases in precipitation in other parts of the basin were predicted to be around 10%. These changes in temperature and precipitation were predicted to reduce the difference between

annual mean precipitation and evapotranspiration (ET) in the northern part of the basin but increase the difference in the southern part of the basin by the end of the 21st century (Shi et al., 2011). Gain et al. (2011) predicted an increase in average and peak streamflow in all seasons, including dry periods, under the A1B and A2 scenarios (Nakicenovic and Swart, 2000).

While these patterns of streamflow were shown to result from climate change, the potential impacts of land use and land cover change were neglected. A substantial increase in future agricultural land is projected for the Brahmaputra basin, possibly through conversion of natural vegetation (e.g., forest) to agricultural land (IMAGE Team, 2001). While clearing the natural vegetation increases surface runoff and river discharge (Costa et al., 2003; Sahin and Hall, 1996), the hydrological response to land use change is not always linear (Ghaffari et al., 2010). Therefore, it is important to account for land use and land cover change along with climate change impacts when predicting long-term patterns in the availability of freshwater.

Potential impacts of future climate and land use change can be quantified for a specific basin by using an integrated hydrological simulation model with downscaled climate and land use projections derived from Global Climate Models (GCM). However, sensitivity assessments with various climate change scenarios can provide valuable insights into the sensitivity of the hydrological systems to changes in climate (Arnell and Liv, 2001), especially in the light of substantial uncertainties in GCM projections (Ficklin et al., 2009; Kirtman et al., 2013). Many large-area integrated hydrological models are currently available; e.g. variable infiltration capacity (Liang et al., 1996), precipitation runoff modeling system (Markstrom et al., 2008), MIKE 11 (Havnø et al., 1995), HEC-RAS (Brunner, 2002). However, the Soil and Water Assessment Tool (SWAT) (Arnold et al., 1998; Gassman et al., 2007) is one of the more widely used models, and we use it in this study.

SWAT allows users to adjust CO_2 concentration, weather parameters (e.g., temperature, precipitation, radiation and humidity), and land use, and includes approaches describing how those parameters affect plant growth, ET, snow, and runoff generation. SWAT has been found to be suitable for large basins such as the Brahmaputra, and has often been used as a tool to investigate climate and land use change effects on freshwater availability around the world (Abbaspour et al., 2009; Gosain et al., 2006; Jha et al., 2006; Montenegro and Ragab, 2010; Rossi et al., 2009; Schuol et al., 2008; Siderius et al., 2013).

The primary goal of this study was to assess long-term patterns of freshwater availability in the Brahmaputra basin under climate and land use and land cover change scenarios. To fulfill the goal, we calibrated the model using the sequential uncertainty fitting II (SUFI2) algorithm (Abbaspour et al., 2004). We then quantified the sensitivity of the hydrological variables such as total water yield, soil water content, ET, streamflow, and groundwater recharge to a group of various climate change scenarios including changes in CO_2 concentration, temperature, and precipitation. We assessed the long-term patterns in the hydrological variables with Phase 3 of the Coupled Model Intercomparison Project (CMIP3) downscaled precipitation and downscaled Integrated Model to Assess the Global Environment (IMAGE) land use change scenarios for the 21st century under the A1B and A2 scenarios (Nakicenovic and Swart, 2000). In brief, the A1B storyline assumes a future world of very rapid economic growth, low population growth, and rapid introduction of new and more efficient technology with the development balanced across fossil fuel and non-fossil fuel energy sources. In contrast, the A2 storyline assumes a very heterogeneous world where population growth is high, economic development is primarily regionally oriented, and per capita economic growth and technological change are more fragmented and slower than in A1B.

2. Study basin

The Brahmaputra is a transboundary river and the world's fourth largest in terms of the average discharge at the mouth, with a flow of ~20,000 $m^3 s^{-1}$ (Jian et al., 2009) (Fig. 1). Originating in the glaciated Kailas range of southern Tibet at 5300 m amsl (above mean sea level), the Brahmaputra traverses 1625 km in China and 918 km in India, before flowing 337 km through Bangladesh and discharging into the Bay of Bengal (Singh et al., 2004). The total drainage catchment of the river is 519,500 km^2 (82°–98° East, and 23°–32° North), of which 50.5% is in China, 33.6% is in India, 8.1% is in Bangladesh and 7.8% is in Bhutan (Immerzeel, 2008). The Tibetan Plateau divides the basin into two distinct climatic zones: (1) the mountain climate, characterized as cold and dry, dominates the

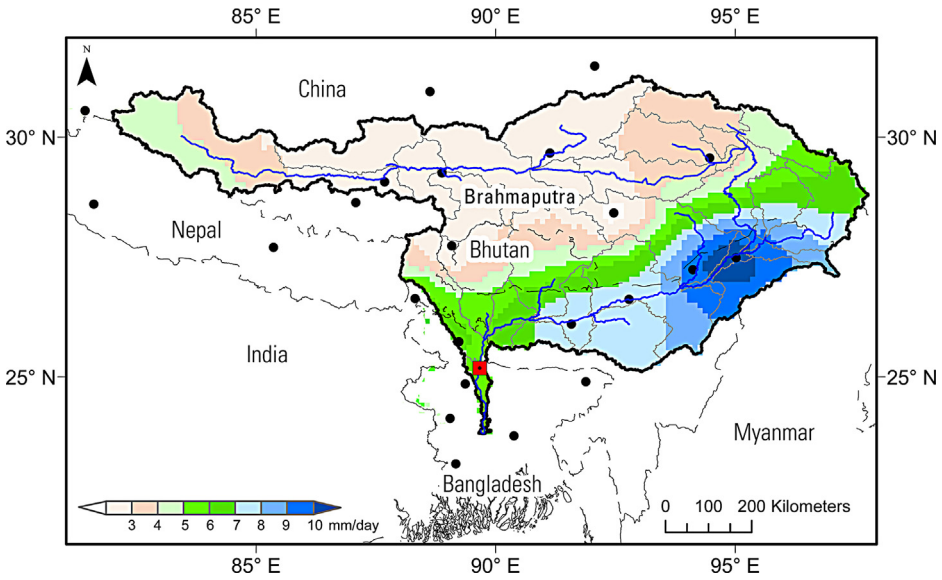

Fig. 1. The Brahmaputra basin along with the subbasins and river overlaid on precipitation climatology (1982–2000). Black dots are observed precipitation stations and the red square is the location of Bahadurabad gauging station in Bangladesh. (For interpretation of the references to color in this legend, the reader is referred to the web version of the article.)

northern part of the basin; and (2) the tropical monsoon climate that dominates the southern part is characterized as warm and humid, and receives high amounts of widespread precipitation, mainly under the influence of the Indian summer monsoon (Singh et al., 2004). The Brahmaputra basin is physiographically diverse and ecologically rich in natural and crop-related biodiversity. The basin is divided into three distinct physiographic zones: (1) the Tibetan Plateau that covers 44.4% of the basin area with elevations above 3500 m amsl, (2) the Himalayan belt that covers 28.6% of the basin area with elevations ranging between 100 and 3500 m amsl, and (3) the lowland floodplains that cover 27% of the basin area with elevations below 100 m amsl (Gain et al., 2011). Average temperature and precipitation in the basin vary by these physiographic zones. Typically, December and January are the coldest months, and the period from May to August includes the warmest months of the year. The average minimum temperature in the Tibetan Plateau drops to −12 °C, and the average maximum temperature varies from 25 °C to 28 °C. In the Himalayan belt, variation in temperature is high because the elevation range is large. In the floodplains, the average minimum temperature is about 9 °C and the average maximum temperature is >35 °C (Singh et al., 2004). Annual average precipitation in the basin is about 1350 mm (Hasson et al., 2013), of which 60–70% occurs during the summer monsoon months of June to September (Gain et al., 2011) when orography plays an important role in the spatial distribution of the precipitation. The basin supports the livelihoods of 66 million people who rely on freshwater for subsistence agriculture (Hasson et al., 2013). Approximately 11% of the basin area is modified for cropland, of which 20% is irrigated (Loveland et al., 2000; Singh et al., 2004).

3. Methods and data used

3.1. SWAT model

SWAT (Arnold et al., 1998; Srinivasan et al., 1998a,b) is a physically based semi-distributed parameter, time-continuous, basin-scale hydrological and agricultural management practice simulation model that runs at a daily time step. The model is also well documented in the literature (Arnold et al., 1998; Ghaffari et al., 2010; Jha et al., 2004b; Sun and Ren, 2013; Ullrich and Volk, 2009). SWAT has been applied in a variety of contexts including: plant growth (Luo et al., 2008), erosion (Tibebe

and Bewket, 2011), nutrient transport and transformation (Jha et al., 2004a), pesticide transport (Luo and Zhang, 2009), sediment transport (Kirsch et al., 2002), water management (Debele et al., 2008), snowmelt (Rahman et al., 2013), land use change (Ghaffari et al., 2010), and climate change impact assessment (Jha et al., 2006). Briefly, in SWAT, a basin is subdivided into multiple subbasins, which are then detailed into hydrological response units (HRUs) based on a unique combination of soil and land use properties. SWAT uses the following water balance equation in the soil profile:

$$SW_t = SW_0 + \sum_{i=1}^{t}(R - Q_{surf} - ET_i - P_i - Q_{gw}) \quad (1)$$

where SW_t is the final soil water content (mm), SW_0 is the initial soil water content on day i (mm), and R, Q_{surf}, ET_i, P_i, and Q_{gw} are daily amounts (mm) of precipitation, runoff, evapotranspiration, percolation, and return flow on day i, respectively, to compute water balance at the HRU level. Flow generation, sediment yield, and nonpoint source loadings are summed across all HRUs in a subbasin, and the resulting loads are then routed through channels, ponds, and/or reservoirs to the basin outlet (Arnold et al., 1998). SWAT simulates hydrological components including ET and canopy storage, soil temperature, mass transport, and management practice from moisture and energy inputs, including daily precipitation, maximum and minimum air temperatures, solar radiation, wind speed, and relative humidity. However, in this study only the hydrological components are discussed. We used the Soil Conservation Service (SCS) curve number procedure to calculate the surface runoff volume. SCS curve number is a value that incorporates soil, land use, and management information (Ficklin et al., 2013). The Penman–Monteith method was selected for ET calculation because it accounts for the effects of changing atmospheric CO_2 in the transpiration computation. Channel routing was simulated using the Muskingum method. The soil percolation component uses a water storage capacity technique to simulate flow through each soil layer in the root zone. Percolation from the bottom of the soil profile recharges the shallow aquifer. Percolation is only allowed when the temperature of the particular layer is above 0 °C. Simultaneously, subsurface lateral flow in the soil profile is calculated on the basis of slope, slope length, and saturated hydraulic conductivity. Groundwater flow contribution to total streamflow is estimated by routing a shallow aquifer storage component to the stream (Arnold et al., 1998).

3.2. Input data and model setup

3.2.1. Weather data

SWAT requires daily precipitation, maximum/minimum air temperature, solar radiation, wind speed, and relative humidity as meteorological inputs. The daily observed precipitation data come from the National Oceanic and Atmospheric Administration (NOAA) Global Surface Summary of Day (GSOD) data set (National Climatic Data Center, 2001). Out of the many available GSOD precipitation stations across the Brahmaputra basin, we carefully selected 23 stations (Fig. 1) to ensure availability of long-term quality observed precipitation records at a daily scale. SWAT accepts one set of weather information for each subbasin. Although these 23 stations were well distributed spatially across the basin, not every subbasin had at least one observing station within it. Therefore, precipitation values from these 23 stations were interpolated using the Inverse Distance Weighting (IDW) method, and the mean areal precipitation was computed for each subbasin at a daily scale. A time-series of the daily mean areal precipitation was compiled for each subbasin. The daily observational records for maximum/minimum air temperature, solar radiation, wind speed, and relative humidity were extracted from the National Centers for Environmental Prediction (NCEP) Climate Forecast System Reanalysis (CFSR) high-resolution coupled atmosphere–ocean–land surface–sea ice system (Environmental Modeling Center, 2010). The CFSR data are provided at points with $0.3^\circ \times 0.3^\circ$ spacing. Data at points closest to the centroid of each subbasin were extracted. The weather information over 16 years (1988–2004) was provided to SWAT as input parameters to produce the observation-driven simulations.

3.2.2. Observed streamflow

The daily observed discharge data at Bahadurabad gauge station were used to calibrate the model parameters in the SWAT Calibration and Uncertainty Programs (SWAT-CUP) and to

validate SWAT observation-driven simulation results. Bahadurabad gauge station is located in northern Bangladesh and less than 200 km upstream from the confluence of the Brahmaputra and the Ganges Rivers. Discharge data have been collected for over 40 years and are maintained by the Bangladesh Water Development Board. These data are of high quality and frequently used in calibration and validation of the basinwide hydrological models (Gain et al., 2011; Immerzeel, 2008; Jian et al., 2009).

3.2.3. Soil and land use data

In addition to weather information, SWAT requires soil properties and land cover information to simulate loads in the hydrological components. The soil map was obtained from the Food and Agriculture Organization of the United Nations (FAO, 1995). At a spatial resolution of 10 km, 106 soil types for the Brahmaputra basin were differentiated, and soil properties for two layers (0–30 cm and 30–100 cm depth) were provided. Other soil properties such as particle-size distribution, bulk density, organic carbon content, available water capacity, and saturated hydraulic conductivity were obtained from Reynolds et al. (1999). The land use and land cover map was obtained from the U.S. Geological Survey (USGS) Global Land Cover Characterization database version 2.0 at 1000 m spatial resolution (Loveland et al., 2000). The original 24 categories were reclassified into 12 to match the land use database of SWAT. Both the soil and land use and land cover maps were resampled to 180 m to correspond to the spatial resolution of the digital elevation model (DEM) used in the simulations.

3.2.4. Model setup

The geographic information system interface – ArcSWAT (Winchell et al., 2010) – was used to parameterize the model for the Brahmaputra basin. The stream network of the basin was delineated from a 180-m DEM resampled from the HydroSHEDS (Hydrological data and maps based on Shuttle Elevation Derivatives at multiple scales) dataset (Lehner et al., 2008). Requiring a minimum drainage area of 12,000 km^2 and including an additional outlet at Bahadurabad discharge gauge station, the basin was subdivided into 29 subbasins. The outlet at the Bahadurabad discharge station constitutes a drainage area of 519,408 km^2. The outlet at Bahadurabad station was considered to be the final outlet of the Brahmaputra basin (Fig. 1). Characterization of the stream reaches and subbasin geomorphology was done automatically by the interface. To further characterize the subbasin for dominant land use and soil types, the multiple Hydrological Response Unit (HRU) option in SWAT was implemented, which resulted in discretization of 527 HRUs for the Brahmaputra basin.

The Brahmaputra is a large basin with diverse elevations. Changes in elevation within the basin strongly influence the snow accumulation and melt process (Pomeroy and Brun, 2001), which can be simulated better when elevation bands and their corresponding subbasin area fractions are defined (Fontaine et al., 2002). To account for the basin's elevation gradient for snow accumulation and melt processes, 10 elevation bands were incorporated at 500-m increments for the maximum allowable range of 2393–6719 m. Accordingly, the percentage of the subbasin area within each elevation band was computed and inserted in the subbasin input file. Out of 29 subbasins, 24 subbasins had fractions of area in multiple elevation bands, and the remaining five subbasins' areas were in a single elevation band.

3.3. SWAT calibration and validation and error assessment

3.3.1. Calibration and validation

The observed precipitation and weather data (temperature, relative humidity, and wind speed) were processed for the period 1988–2004. The year 2002 was excluded due to missing records in the GSOD precipitation. The period 1988–1997 was used to calibrate the model, and 1998–2004 (excluding 2002) was used to validate the model. The first 2 years for each simulation were used for model spin-up time, which were, as well as the missing data year of 2002, excluded from subsequent analyses. We calibrated the SWAT model at the basin level using observed river discharge at the Bahadurabad discharge station. Before running the calibration, we analyzed the sensitivity of the parameters by using

Table 1
The sequential uncertainty fitting (SUFI2) optimized value with optimization range of the SWAT model parameters included in the final calibration.

Parameters	Description with unit	Fitted value	Calibration range	
			Min	Max
*r*_CN2	SCS curve number for moisture condition II	2.15%	−10%	10%
*v*_ESCO	Soil evaporation compensation factor	0.69	0.05	1
*v*_ALPHA_BF	Baseflow alpha factor (days)	0.064	0	0.30
*v*_PLAPS	Precipitation lapse rate (mm H_2O/km)	172.25	50	300
*v*_TLAPS	Temperature lapse rate (°C/km)	−5.50	0	−6
*v*_SLSUBBSN	Average slope length (m)	−0.60	0.05	1
*a*_GWQMN	Threshold depth of water in the shallow aquifer required for return flow to occur (mm H_2O)	8.26	0	200
*a*_REVAPMN	Threshold depth of water in the shallow aquifer required for revap or percolation to the deep aquifer to occur (mm H_2O)	4.35	0	15
*a*_GW_REVAP	Groundwater 'revap' coefficient	0.01	0.01	0.10
*v*_EPCO	Plant uptake compensation factor	0.38	0	1

"*r*_" means the existing parameter value is multiplied by (1 + *a* given value), "*v*_" means the default parameter is replaced by the given value, and "*a*_" means the given parameter value is added to the existing parameter value.

the Latin hypercube one-factor-at-a-time (LH-OAT) method of SWAT (van Griensven et al., 2006). This approach combines the advantages of global and local sensitivity analysis methods and can efficiently provide a rank ordering of parameter importance (Sun and Ren, 2013). Based on sensitivity, the top-ranked 10 sensitive parameters (Table 1) were optimized using the SUFI2 algorithm in the SWAT-CUP. In SUFI2 all uncertainties such as model input, model conceptualization, model parameters, and measured data are mapped onto the parameter ranges as the procedure tries to capture most of the measured data within the 95% prediction uncertainty (Abbaspour et al., 2009). Overall uncertainty in the output is quantified by the 95% prediction uncertainty (95PPU) calculated at the 2.5% and 97.5% levels of the cumulative distribution of an output variable obtained through Latin hypercube sampling. The goodness of calibration/uncertainty performance is quantified by *P*-factor, which is the percentage of data bracketed by the 95PPU band, and *R*-factor, which is the average width of the band divided by the standard deviation of the corresponding measured variable. Thus, SUFI2 seeks to bracket most of the measured data within the smallest possible uncertainty band (Abbaspour, 2007). During calibration, our target was to bracket most of the measured data including uncertainties within the 95PPU band, a *P*-factor close to 1, while having the narrowest band, an *R*-factor close to zero. The other indices of performance available in SWAT-CUP, including the coefficient of determination (R^2), Nash–Sutcliffe (NS) (Nash and Sutcliffe, 1970), and br^2 (R^2 times the slope), were also considered when assessing the goodness of fit between the observation and the best simulation.

The calibrated model was run for the period 1998–2004 for validation by keeping the optimized parameters constant and allowing only the observed precipitation to vary. The calibrated and validated model was run for the entire time period 1988–2004 under an average atmospheric CO_2 concentration of 330 ppm. These simulation results were used as the baseline scenario.

3.3.2. Error assessment

The ability of the SWAT model to simulate streamflow was evaluated using four complementary measures of model performance: (1) percent bias, (2) R^2, (3) Nash–Sutcliffe model efficiency coefficient (NS), and (4) root mean square error (RMSE). The equations describing these measures are provided in Appendix A.

Table 2
Various changes in CO_2 concentration, temperature, and precipitation for sensitivity scenarios.

Scenarios	Modified climate inputs		
	CO_2 (ppmv)	Temperature change (°C)	Precipitation change (%)
Baseline	330	0	0
1 (1.5×)	495	0	0
2 (2×)	660	0	0
3	330	+2	0
4	330	+4	0
5	330	0	+10
6	330	0	+20

4. Model experimental design, precipitation, and land use projections

4.1. Experimental design

The baseline scenario was assumed to reflect current conditions. To evaluate the magnitude of responses from the hydrological systems of the Brahmaputra basin to various components of climate change, we designed six scenarios by altering one variable at a time. These scenarios are presented in Table 2. Each scenario was run for the same simulation period (1988–2004), except with modified climatic inputs, which provided a consistent basis for the scenario impacts as compared to baseline conditions. Although a 30-year period is preferred to present baseline conditions (Arnell, 1996; Jha et al., 2006), we used a 15-year period (1988–2004) including three major flooding years (1988, 1998 and 2004) and two major drought years (1989 and 1994) for the baseline because of the limitations in the station observed precipitation data. The sensitivity simulations were designed based on the approach described in Jha et al. (2006) and Wu et al. (2012b). The first two simulations in Table 2 focused on multiplying the baseline daily atmospheric CO_2 concentration by factors of 1.5 and 2.0, which are within the range of atmospheric CO_2 projections described in the Fourth Assessment Report (AR4) of the Intergovernmental Panel on Climate Change (IPCC) for the region, but less than the projections described in the Fifth Assessment Report (Kirtman et al., 2013; Solomon, 2007). The next two simulations reflected a daily increase in minimum and maximum air temperature by 2 °C and 4 °C incorporated in the baseline scenario. The CMIP5 multi-model mean projection of the annual average temperature change over south Asia was over 3 °C (Hijioka et al., 2014). The last two scenarios represented 10% and 20% increases in the daily precipitation over the baseline scenario. The CMIP5 multi-model mean projected a precipitation increase up to 12% over south Asia by the end of the 21st century which was similar to the projections by the CMIP3 models (Kirtman et al., 2013; Shashikanth et al., 2013).

Next, we designed future climate and land use change impact assessment simulations with estimated CO_2 concentration, temperature increase, and land use change scenarios for each 10-year period of the 21st century. The scenarios were executed with third-generation Canadian GCM version 3.1 (CGCM3.1) Statistical Downscaling Model (SDSM)-downscaled precipitation (Pervez and Henebry, 2014), projected temperature and CO_2 concentration, and downscaled IMAGE-projected land use information for the A1B and A2 scenarios. The simulation results were used for the long-term evaluation of the basin's freshwater availability. One additional simulation for a 15-year period (2060–2075) was included and the results were used to investigate hydrological consequences compared to the baseline scenario. Projected CO_2 concentration and temperature is provided in Table B1.

4.2. Downscaling of land use projections

The changes in agricultural land areas were modeled in IMAGE, version 2.2 (IMAGE Team, 2001), because the model is capable of forecasting land use change based on the joint modeling of human activities and environmental processes (Dobrovolski et al., 2011). IMAGE mapped agricultural land

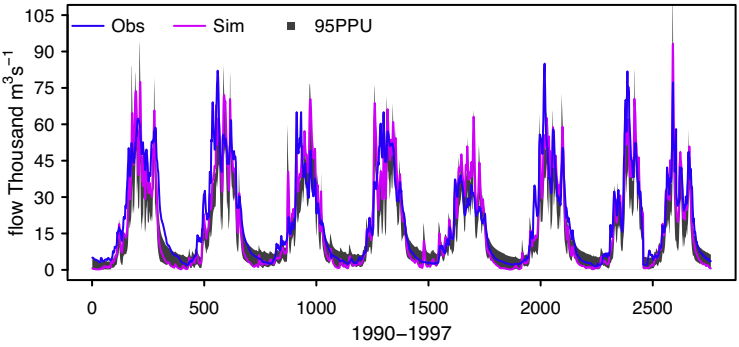

Fig. 2. Simulated daily streamflow at Bahadurabad station for the period 1990–1997. Gray shaded area is the uncertainty in the simulated daily streamflow quantified by the 95% prediction uncertainty.

areas on a grid of $0.5^\circ \times 0.5^\circ$ spatial resolution; therefore, the output cannot be directly used as future agricultural land requirements. To downscale these projections, we weighted the actual IMAGE projections using a scenario change factor (Sleeter et al., 2012) computed from IMAGE agricultural area projection and the agricultural area estimate provided by a USGS global land cover dataset (Loveland et al., 2000).

4.3. Downscaling of precipitation

GCMs are considered to be the most appropriate means for projecting climate change. However, due to their coarse spatial resolution, it is essential to use downscaled GCM outputs rather than raw output for impact studies (Chu et al., 2010; Wilby et al., 1999), because local scale forcings, processes, and feedbacks are not well represented in GCM experiments (Hewitson and Crane, 2006; Wetterhall et al., 2009). We used statistically downscaled precipitation for both A1B and A2 scenarios on the basis of empirical statistical relationships established in the SDSM (Wilby et al., 2002) between historical (1988–2004) large-scale circulation patterns and atmospheric moisture variables from the NCEP reanalysis dataset (Kalnay et al., 1996) and locally observed precipitation from the GSOD dataset for the same time period (Pervez and Henebry, 2014). The 21st century daily precipitation was then modeled through a stochastic weather generator applying the established relationships with the probability of the precipitation depending on CGCM3.1 predictor variables. The comparison of observed precipitation with CGCM3.1 projected raw and downscaled precipitation concluded that downscaled precipitation provided consistency and attenuated uncertainties while simulating future precipitation (Pervez and Henebry, 2014). The precipitation was downscaled at the subbasin level and daily time-series were created and assigned to each subbasins' centroid to be used in the calibrated SWAT model.

5. Results

5.1. SWAT model calibration, validation, and uncertainty analysis

Fig. 2 illustrates the daily observed and simulated streamflow at Bahadurabad station. The shaded gray regions indicate 95% prediction uncertainty (95PPU) by the simulation. The *P*-factor was 0.78, which signifies that 78% of the observed daily streamflow could be bracketed by the uncertainties. The *R*-factor (average thickness of 95PPU divided by standard deviation) was 0.64. Although an *R*-factor of 0 is desirable, a value close to 1 is considered reasonable (Abbaspour et al., 2009; Schuol et al., 2008). However, uncertainties were relatively high during low flow seasons, which can be seen as a model deficiency in simulating groundwater flow (Rostamian et al., 2008). The model performance metric

Table 3
Model calibration and validation statistics for streamflow at the Bahadurabad station.

Type	Period	Time scale	Mean streamflow ($m^3 s^{-1}$)		Bias (%)	R^2	NS	RMSE ($m^3 s^{-1}$)
			Observed	Simulated				
Calibration	1988–1997	Annual	22,731	21,437	−3.2	0.85	0.85	7089
Validation	1998–2004	Annual	20,880	19,744	−4.4	0.89	0.88	5387
Baseline	1988–2004	Annual	22,345	22,875	2.9	0.77	0.73	9089

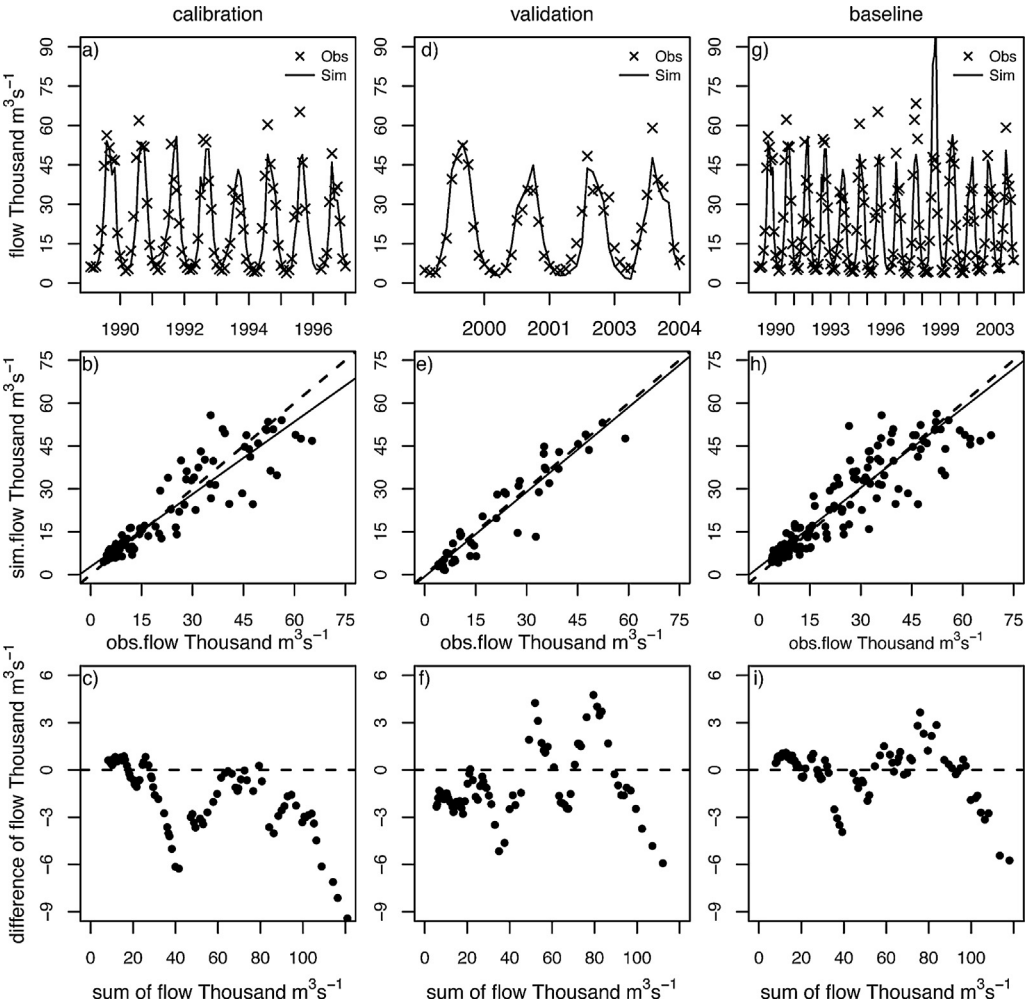

Fig. 3. Comparison of monthly observed and simulated streamflow at Bahadurabad station for calibration (1990–1997), validation (2000–2004), and baseline (1990–2004) periods.

values in Table 3, and *P*-factor, and *R*-factor indicate the model is reliable in simulating Brahmaputra basin streamflow.

Graphical comparisons of observed and simulated streamflow at a monthly scale for calibration (1988–1997), validation (1998–2004), and baseline (1988–2004) periods are shown in Fig. 3. In general, the model accurately tracked the observed streamflow for the time periods, although some peak

flow months were underpredicted during calibration, but the under-prediction was less during validation, possibly due to less temporal variability in the precipitation. Monthly flow statistics in Table 3 suggest a strong correlation between simulated and observed streamflow in all three periods. The NS coefficients for simulated streamflows were 0.85, 0.88, and 0.73 for the calibration, validation, and baseline periods, respectively. These coefficients suggest that model performance for monthly streamflow was relatively better than daily. The model underpredicted streamflows for the calibration and validation periods by 3.2% and 4.4%, respectively. The regression lines and sum difference plots reveal that the underprediction occurred primarily during higher flows (Fig. 3b, c, e, and f). Literature suggests that SWAT is not designed to simulate extreme events and the model usually underpredicts the largest flow events (Chu and Shirmohammadi, 2004; Tolson and Shoemaker, 2004). However, a positive bias for simulated streamflow of 2.9% was noticeable for the baseline. The notable 1999 overprediction of peak flow may have contributed to this positive bias in simulated streamflow. Overall, the SWAT model was able to simulate well the actual hydrological conditions in the Brahmaputra basin.

5.2. Evaluation of parameterization

Ten sensitive parameters were used to calibrate the model (Table 1). These parameters primarily represented surface runoff, groundwater, snow, ET, and the routing process for the basin's hydrology. The values for the following parameters were found to be commonly used in other studies to calibrate the SWAT model: CN2 (SCS runoff curve number for moisture condition II), ESCO (soil evaporation compensation factor), ALPHA_BF (baseflow alpha factor), SLSUBBSN (average slope length), GWQMN (threshold depth of water in the shallow aquifer required for return flow to occur), and GW_REVAP (ground revap coefficient) (Cibin et al., 2010; Ghaffari et al., 2010; Heuvelmans et al., 1999; Mutenyo et al., 2013; Wu et al., 2012a). While the final fitted values were optimized by the automatic calibration algorithm SUFI2, the values were checked for correspondence to the basin characteristics and their underlying hydrological processes. The average CN2 value was 61. The baseflow alpha factor value of 0.064 was considered to be small, which suggests slow drainage and high storage in the basin's shallow aquifer. The adjusted EPCO (plant uptake compensation factor) value of 0.38 indicated that most water used by vegetation would be from the upper soil profile because of a relatively higher groundwater table, sufficient soil moisture, and limited transpiration. The ESCO value of 0.69 also indicated that more water was being extracted from the upper level to compensate for the evaporative demand. A good calibration is most likely a combined effect from all selected parameter coefficients. However, the sensitivity of individual parameters varies. Because of snow and diverse elevations, the temperature and precipitation lapse rates were found to be important in simulating the hydrological processes in the Brahmaputra basin. The optimized temperature lapse rate was $-5.5\,^{\circ}$C per 1-km rise in elevation, which was found in agreement with temperature lapse rate between $-5\,^{\circ}$C to $-7\,^{\circ}$C per 1-km elevational rise used in other studies (Baral et al., 2014; Thayyen et al., 2005). Precipitation in the Himalayan region clearly varies with elevation (Bookhagen and Burbank, 2006), although the precipitation elevation relationship is not always linear (Immerzeel et al., 2014). Precipitation was observed to increase at a rate of 150 mm per 1-km rise in elevation in the valleys with elevations between 1396 and 2492 m; Precipitation then decreased at a rate of 240 mm per 1-km rise in elevation between the elevation range of 3539–3875 m, and then increased again at a rate of 60 mm per 1-km rise in elevation between 3981 and 5100 m (Baral et al., 2014). It was also reported that precipitation decreased with an increase in elevation in very high elevation regions in the Himalayas (Immerzeel et al., 2014). However, SWAT incorporates the PLAPS variable to account for the precipitation lapse rate as a global variable and does not allow incorporation of PLAPS values by elevation bands; therefore, the SUFI2 optimized precipitation lapse rate of 172.25 was used as a universal value for all elevation bands. This limitation can be considered a weakness of the SWAT model. The low 8.26 value of GWQMN helped increased the baseflow, while the value of 0.01 for GW_REVAP facilitated the increase in baseflow by decreasing the water transfer from the shallow aquifer to the root zone, which was necessary to simulate flow during the low flow seasons.

Table 4
Average monthly estimates of the observed (precipitation, minimum and maximum temperatures) and simulated hydrological components (streamflow, water yield, soil water content, ET, and groundwater recharge) for the baseline scenario.

Month	Observed				Simulated			
	Precip. (mm)	Min temp (°C)	Max temp (°C)	Streamflow ($m^3 s^{-1}$)	Water yield (mm)	Soil water content (mm)	ET (mm)	Groundwater recharge (mm)
Jan	23	−6.3	6.8	6259	9	117	11	−3
Feb	32	−4.9	7.8	5552	6	119	15	2
Mar	53	−1.0	11.8	6191	15	120	28	7
Apr	100	3.0	14.7	9125	35	123	48	14
May	180	6.7	17.4	15,998	94	126	67	24
Jun	325	10.3	19.8	29,643	184	130	75	47
Jul	399	12.1	20.5	47,613	264	140	82	43
Aug	364	12.0	20.0	49,338	265	145	80	16
Sep	260	9.9	18.3	47,000	216	146	66	−17
Oct	86	4.4	14.5	32,804	121	138	42	−58
Nov	16	−1.8	10.9	15,765	49	125	21	−42
Dec	10	−5.8	7.8	9214	21	118	13	−18
Annual	1849	3.2	14.2	22,875	1279	129	548	15

5.3. Characteristics of the baseline scenario

The observed and simulated estimates of the hydrological components for the 16-year baseline period are provided in Table 4. The average annual total observed precipitation was 1849 mm. The annual average simulated streamflow at Bahadurabad gauge station was 22,875 $m^3 s^{-1}$, which was slightly larger than the average observed streamflow (22,345 $m^3 s^{-1}$) for the same period (Table 3). The average daily observed minimum and maximum temperature was 3.2 °C and 14.2 °C, respectively. The average annual total water yield from the baseline simulation was 1279 mm. The total water yield is the total amount of water produced in the HRU that enters the main channel, which essentially is the sum of surface runoff, lateral flow, and return flow minus the transmission loss (water lost from tributary channels in the HRU via transmission through the bed). Average annual ET was 548 mm, average monthly soil water content was 129 mm, and the average annual groundwater recharge was 15 mm. In addition to the estimates provided in Table 4, the annual average transmission loss was 11.41 mm and groundwater revap (movement of water from shallow aquifer back to the overlying unsaturated zone) was 7.55 mm. Although the transmission loss and groundwater revap are considered minor components of the overall hydrological balance (Jha et al., 2006), they are important in equalizing the water balance. The amount of water lost through transmission becomes recharge for the shallow aquifer therefore can be added to groundwater recharge; whereas, the groundwater revap accounts for water that moves from the shallow aquifer into the overlying unsaturated zone and, thus, needs to be subtracted from the groundwater recharge. In equalizing the water balance during the baseline period, the annual average basin water output was computed as the summation of water yield, ET, groundwater recharge, and transmission loss minus the groundwater revap, which was equal to 1846 mm compared to the average annual input precipitation of 1849 mm. The 3-mm difference between the input and output of water in the water balance could be attributed to 1-mm gain in the soil water content at the end of the cycle (Table 4) and to rounding of the numbers in Table 4.

5.4. CO_2, temperature, and precipitation sensitivity scenarios

5.4.1. Increase in CO_2 concentration

The first two runs from Table 2 simulated the influence of a 1.5× and 2× increase in CO_2 concentration on the basin's hydrological components. The total water yield and soil water content was predicted to increase with higher CO_2 concentration (Fig. 4a and b). The annual total water yield was predicted to increase by 2% and 5% in response to a 1.5× and 2× increase in CO_2 concentration, respectively (Table 5). While total water yield increased in every month, the predicted increase was more

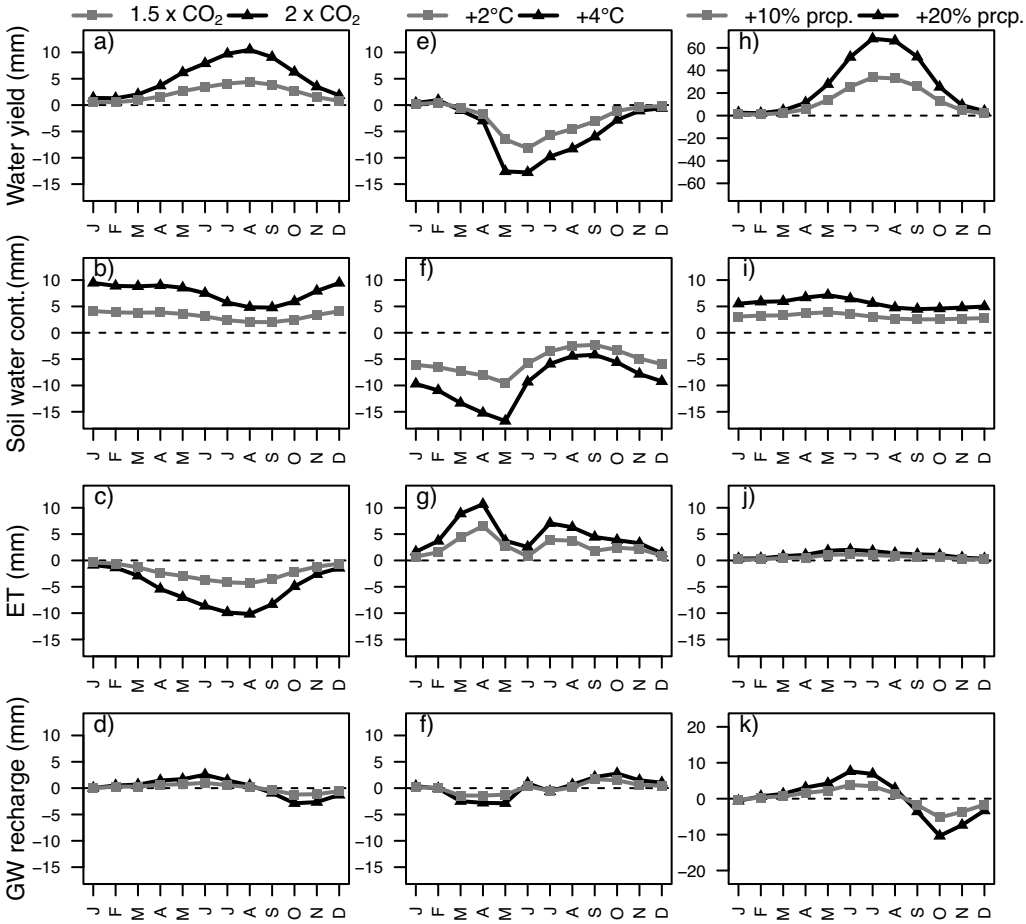

Fig. 4. Anomalies of the simulated annual cycle of total water yield, soil water content, evapotranspiration (ET), and groundwater recharge by month in response to various changes in CO_2 concentration, temperature, and precipitation.

Table 5
Average annual percent change (%) of hydrological components compared to the baseline scenario in response to various changes in CO_2 concentration, temperature, and precipitation.

Hydrological components	CO_2 (ppmv)		Temperature		Precipitation	
	495 (1.5×)	660 (2×)	+2 °C	+4 °C	+10%	+20%
Total water yield	2	5	−2	−4	13	25
Soil water content	3	6	−4	−7	2	4
ET	−5	−12	6	10	1	2
Streamflow	3	6	−3	−5	13	27
Groundwater recharge	3	8	−3	−6	9	18

pronounced during the summer monsoon months of June through September. Fig. 4c indicates that the ET was predicted to decrease, with the largest decrease occurring between June and November. The average annual ET was predicted to decline by 12% with 2× CO_2 (Table 5). Increased CO_2 concentration has profound impacts on plant physiology (Sellers et al., 1996) through the reduced opening of the plant stomata known as physiological forcing (Field et al., 1995). Physiological forcing can reduce ET (Betts et al., 1997; Hungate et al., 2002; Stockle et al., 1992), ET and reduced ET leaves more water in

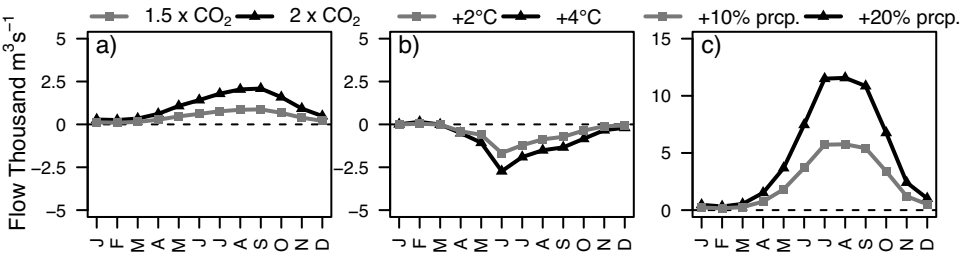

Fig. 5. Anomalies of the simulated annual cycle of streamflow by month in response to various changes in CO_2 concentration, temperature, and precipitation.

the soil profile, increasing the soil water content. Moisture soils can raise the water yield (Ficklin et al., 2009) by generating more surface runoff, lateral flow, and seepage, all of which contribute to increasing streamflow (Wu et al., 2012b). Our simulations with increased CO_2 concentration predicted 3% and 6% increases in annual average streamflow in response to a 1.5× and 2× increase in CO_2 concentration, respectively (Fig. 5a and Table 5). The increase in streamflow due to physiological forcing agrees with other research. River runoff was observed to increase continentally during the 20th century, and continental runoff was predicted to increase by 6% globally from physiological forcing due to a 2× concentration in CO_2 (Betts et al., 2007; Gedney et al., 2006). Predicted reduced ET, increased soil water content, and increased total water yield eventually may lead to 3% and 8% increases in average annual groundwater recharge in response to a 1.5× and 2× increase in CO_2 concentration (Fig. 4d and Table 5).

5.4.2. Increase in temperature

Changes in ET were more pronounced in response to 2 °C and 4 °C increases in temperature. The average annual ET was predicted to increase by 6% and 10%, respectively, with the maximum increase occurring during the spring months (Fig. 4g). The predicted increase in ET resulted in a decrease in soil water content, total water yield, and groundwater recharge (Fig. 4e, f, and h). The maximum 13% predicted relative decrease in soil water content was in May, following the peak predicted ET in April. The drier soil reduced the water yield and the groundwater recharge as it affected surface runoff, lateral flow, and baseflow (Table 5). Although the predicted average annual total water yield decreased in response to temperature increase, it was predicted to increase for January and February. A similar pattern was also evident for the predicted streamflow in response to changes in temperature. While average annual streamflow was predicted to decrease by 3% and 5%, a noticeable increase of 4.7% and 17.5% in streamflow was predicted for the month of February in response to 2 °C and 4 °C increases in temperature, respectively (Fig. 5b). The predicted increase in winter months' streamflow and total water yield signified the basin's sensitivity to the effect of a decrease in snowpack level and successive increase in snowmelt runoff.

5.4.3. Increase in precipitation

Precipitation is the key input to the hydrological cycle. Consistent linear increases in total water yield, soil water content, ET, streamflow, and groundwater recharge were predicted in response to 10% and 20% increases in precipitation (Figs. 4h–k and 5c). With a 10% increase in precipitation, average annual streamflow was predicted to increase by 13%, and with a 20% increase in precipitation, average annual streamflow was predicted to increase by 27% (Table 5). The increase was more pronounced in the summer monsoon months of June through September (Fig. 5c). Changes in streamflow were the highest among all the hydrological components we studied. The standard deviation of the monthly streamflow was 2.5 for a 10% precipitation increase, and 5.3 for a 20% precipitation increase, which indicated that variability in streamflow increased with increasing precipitation. The average annual total water yield was predicted to increase by 13% and 25%, and the average monthly soil water content was predicted to increase by 2% and 4%, and groundwater recharge was predicted to increase by 6% and 10% in response to 10% and 20% increases in precipitation, respectively. Predicted increases in average annual ET were among the lowest, between 1% and 3% for the 10% and 20% increases, respectively.

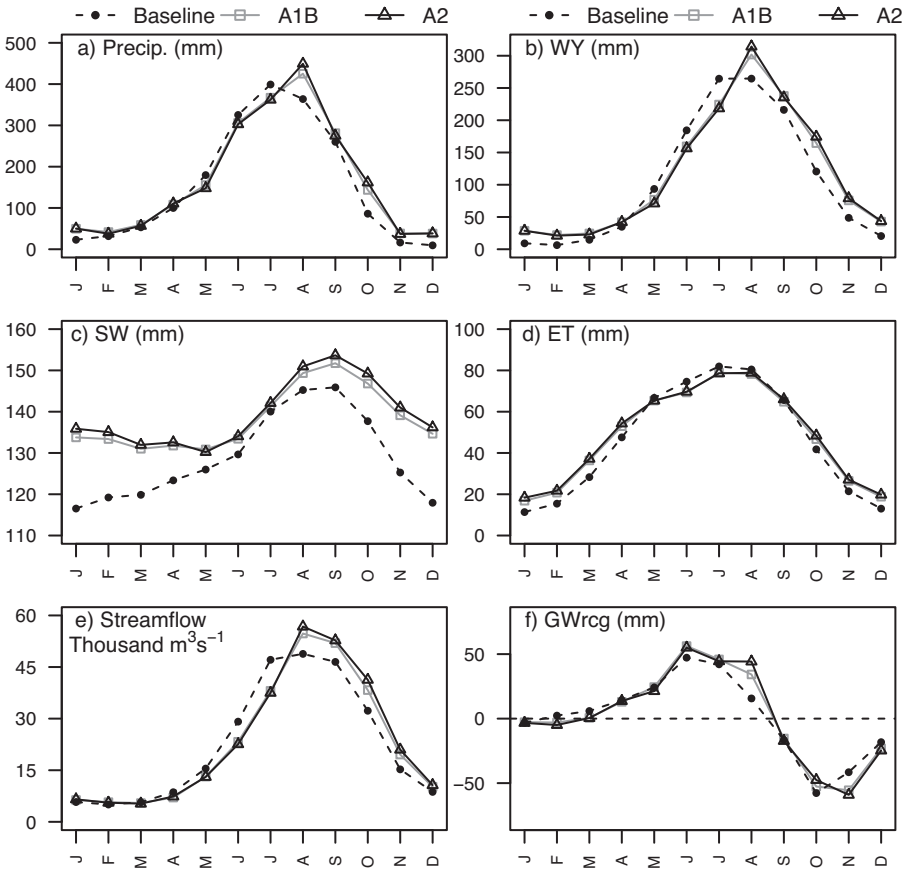

Fig. 6. Comparison of basin-wide monthly observed and simulated (a) precipitation (precip.), (b) total water yield (WY), (c) soil water content (SW), (d) evapotranspiration (ET), (e) streamflow, and (f) groundwater recharge (GWrcg) between the baseline period (1988–2004) and the projected period (2060–2075) under the A1B and A2 scenarios.

5.5. Climate and land use change impact scenarios

We applied the SDSM downscaled CGCM3.1 precipitation outputs with the projected CO_2 concentration, temperature, and land use change into the SWAT model to investigate hydrological effects of potential future climate and land use change for the 21st century. In addition, a separate simulation

Table 6
Seasonal average percent change (%) of the hydrological components for the period 2060–2075 compared to the baseline scenario.

Period	Precipitation (%)		Water yield (%)		Soil water content (%)		ET (%)		Streamflow (%)		GW recharge (%)	
	A1B	A2	A1B	A2	A1B	A2	A1B	A2	A1B	A2	A1B	A2
MJJ	−8	−10	−15	−18	2	3	−4	−4	−19	−20	11	6
ASO	20	25	17	20	4	6	1	3	14	18	42	65
NDJ	157	156	86	91	13	15	35	42	21	28	−29	−38
FMA	13	11	58	54	9	10	21	24	−6	−6	−52	−59
Annual	9	10	9	10	7	8	5	7	2	4	47	49

MJJ: May, June, July; ASO: August, September, October; NDJ: November, December, January; FMA: February, March, April.

was executed for a 15-year period (2060–2075) to analyze climate and land use change impacts on the hydrological components for a time slice 50 years from now.

An increase in agricultural land of up to 42% is expected by 2070 followed by a reduction to 36% by 2100 under the A1B scenario. In contrast, a continuous increase to 76% was expected under the A2 scenario by the end of the 21st century. It has been estimated that up to 11.9% (for A1B) and 22.8% (for A2) of each existing land cover type needs to be converted to agriculture to offset the expected increase in agricultural land. Projected changes in land use and the corresponding land cover conversion requirements are presented in Table A2 in Appendix B. The expected changes in land use based on Table B2 have been implemented in the SWAT for the respective time periods during the simulations.

The basin average monthly baseline (1988–2004) and projected precipitation for the period (2060–2075) are presented in Fig. 6a. The average annual precipitation in the Brahmaputra basin was predicted to increase from 1849 mm to 2013 mm and 2029 mm, a 9% and 10% increase compared to baseline precipitation under the A1B and A2 scenarios, respectively. The annual precipitation cycle was expected to remain the same, with the June through September monsoon having the highest precipitation in the year, although predicted relatively high (>60% increase) precipitation during October (Fig. 6a) suggests an extension in monsoon could be possible. Wetter projections and a possible extension in the monsoon precipitation corroborates well with earlier studies (Annamalai et al., 2007; Kripalani et al., 2007; Sabade et al., 2011). Changes in the seasonal distribution of the precipitation were also predicted. Precipitation during the early monsoon months of May, June, and July was predicted to decrease by 8% and 10%, while the August, September, and October precipitation was predicted to increase by 20% and 25%, respectively, under the A1B and A2 scenarios (Table 6). The peak monsoon precipitation was predicted to shift from July to August with an expected additional 61 mm (17%) and 85 mm (23%) of precipitation in August alone under the A1B and A2 scenarios, respectively. A similar shift in peak monsoon precipitation over south Asia due to climate change was predicted by Kripalani et al. (2007). A more than two-fold increase in November through January precipitation was also predicted by 2075; however, that increase will have limited influence on the annual hydrological budget because November to January accounts for only 6% of the annual precipitation. The predicted changes in the Brahmaputra precipitation over the 21st century by 25-year epoch presented a similar pattern for annual cycle and magnitude of the change (Pervez and Henebry, 2014).

The impacts of climate and land use change on the hydrological components of the Brahmaputra basin are presented in Fig. 6b–f. In response to an expected increase in annual precipitation, the loadings in the hydrological components were predicted to increase annually with seasonal variability relative to the baseline (Table 6). Under the A1B and A2 scenarios, the total water yield was projected to increase by 9% and 10% annually. Fig. 6b indicates an increase in total water yield in all seasons except the early monsoon months of May, June, and July. During this period, total water yield was predicted to decrease principally because of a decrease in precipitation and an increase in temperature. May through July accounts for 33% of the annual total water yield; therefore, 15% and 18% predicted decreases in water yield will potentially increase the drought risk during these months under the A1B and A2 scenarios, respectively (Table 6). Later in the monsoon, August, September, and October, total water yield was projected to increase by 17% and 20% under the A1B and A2 scenarios, respectively. August through October is the wettest period of the year, accounting for 51% of the annual water yield. An increase in water yield will potentially elevate the flooding risk between August and October in the basin. Water yield was expected to increase over the dry period from November to April, which might be helpful to mitigate the prevailing dry conditions in those months.

The climate and land use change impacts on soil water content was predicted to increase by 7% and 8% annually, with most of the increase being predicted during November to January (13% and 15%) and the smallest increase being predicted during May to July (2% and 3%) under the A1B and A2 scenarios, respectively (Fig. 6c). Increased soil water content and increased temperature would potentially increase ET in the basin. ET was projected to increase annually by 5% and 7% for the A1B and A2 scenarios, respectively; however, it was predicted to decrease during the early monsoon months of May through July by about 4%, primarily because of the combined influence of reduced precipitation and increased physiological forcing (Fig. 6d). In contrast, average ET was predicted to increase by 12% and 14% due to increased soil water content and temperature between August and April under the A1B and A2 scenarios, respectively. These findings indicated that the key drivers for ET varied by season:

while it was physiological forcing during the early monsoon months; it was the temperature and soil water content for the rest of the year.

Although the climate and land use change scenario impacts yielded relatively low increases of 2% and 4% in the annual streamflow of the Brahmaputra River, the large variations in seasonal streamflow relative to the baseline were predicted by the SWAT model, confirming that the seasonal variability would increase as a result of changes in climate and land use (Table 6). Streamflow was predicted to decrease by 6% during the pre-monsoon months of February through April, and decrease by 19% and 20% during the early monsoon months of May through July under the A1B and A2 scenarios, respectively. These results agreed with the findings of Immerzeel et al. (2010) for the A1B scenario, but contradicted the findings of Gain et al. (2011), who predicted increased streamflow in all seasons for both A1B and A2 scenarios. The predicted decrease in streamflow during the dry period implied that the effects of ET become more pronounced than glacial melt and snowmelt during the dry period. In contrast, compared to the baseline scenario, streamflow was projected to increase by 14% and 18% during August through October and by 21% and 28% during November through January under the A1B and A2 scenarios, respectively (Table 6). The greatest differences were predicted to occur during the peak monsoon months of July and August. July streamflow was predicted to decrease by 19% (47,113–38,082 $m^3 s^{-1}$) and 20% (47,113–37,490 $m^3 s^{-1}$), and August streamflow was predicted to increase 12% (48,838–54,739 $m^3 s^{-1}$) and 16% (48,838–56,761 $m^3 s^{-1}$) under the A1B and A2 scenarios, respectively, compared to the baseline. These changes agree with the findings of previous research (Immerzeel, 2008) under the A2 scenario. The streamflow between November and January was predicted to increase from an average of 9913–12,038 $m^3 s^{-1}$, and 12,727 $m^3 s^{-1}$ under the A1B and A2 scenarios, respective increases of 21% and 28% compared to the baseline. The winter streamflow was also predicted to increase in the Brahmaputra basin under the A1B and A2 scenarios (Gain et al., 2011). These relatively large predicted increases during the winter months could possibly be the result of increased snowmelt and more precipitation in the form of rainfall due to the increase in winter temperature. Similar climate change impacts in winter streamflow were also reported for the upper Mississippi River basin in the United States (Jha et al., 2006).

The substantial projected increases in water yield, soil water content, and streamflow as impacts of climate and land use change yielded increased groundwater recharge in the Brahmaputra basin (Fig. 6f). The groundwater recharge was predicted to increase by 47% and 49% annually under the A1B and A2 scenarios, respectively (Table 6).

5.6. Trends in projected freshwater availability

Simulation results for the climate and land use change scenarios were summarized to assess long-term response patterns of the hydrological components. Monthly estimates of hydrological components were averaged for the early part of the monsoon season from May through July (MJJ), the later part of the monsoon season from August through October (ASO), as well as two other 3-month periods: November through January (NDJ), and February through April (FMA). Trends were determined using the nonparametric Mann–Kendall trend test, and the corresponding z scores and p values are presented in Table 7. Fig. 7 shows both the average percentage change from long-term average (as percent on left ordinate) and the average quantity (on right ordinate) for the total water yield (mm), soil water content (mm), groundwater recharge (mm), and streamflow (thousand $m^3 s^{-1}$) in four 3-month periods MJJ, ASO, NDJ and FMA. A significant decreasing trend in the total water yield during MJJ was predicted for the 21st century under both A1B and A2 scenarios with the average water yield remaining below the baseline (Fig. 7a). The trend appeared in direct response of the predicted decrease early monsoon precipitation in the basin (Fig. 6a). Thereafter, increasing trends in the total water yield were predicted for the other periods (Fig. 7b–d) (Table 7). The noticeable projection range of total water yield was from 211 mm to 261 mm (5–30% increase from the baseline) during ASO, and it was from 43 mm to 50 mm (20–40% increase from the baseline) during NDJ. In contrast, the long-term patterns of the soil water content showed little change (Fig. 7e–h) – in the range between 147 mm and 165 mm (3–15% increase from the baseline), which may result from the limited water-holding capacity of the soils (Wu et al., 2012b). The long-term patterns in the streamflow responded directly to total water yield for the basin. A significant strong decreasing trend in MJJ streamflow was

Table 7
Projected trends in hydrological components for the Brahmaputra basin based on Mann–Kendall trend test.

Period	A1B								A2							
	Water yield		Soil water content		Streamflow		Groundwater		Water yield		Soil water content		Streamflow		Groundwater	
	z	*p*-Value	*z*	*p*-Value	*z*	*p*-Value	*z*	*p*-Value	*z*	*p*-Value	*z*	*p*-Value	*z*	*p*-Value	*z*	*p*-Value
MJJ	−10.0	<0.001	−0.8	0.429	−6.7	<0.001	−9.6	<0.001	−10.7	<0.001	7.1	<0.001	4.6	<0.001	−11.7	<0.001
ASO	7.4	<0.001	6.9	<0.001	9.3	<0.001	7.3	<0.001	7.2	<0.001	6.5	<0.001	9.9	<0.001	11.8	<0.001
NDJ	5.1	<0.001	6.0	<0.001	9.9	<0.001	−1.5	0.133	8.8	<0.001	4.7	<0.001	10.2	<0.001	−9.6	<0.001
FMA	3.5	<0.001	0.1	0.906	6.2	<0.001	2.1	0.036	4.7	0.012	0.0	0.995	6.1	<0.001	6.5	<0.001

MJJ: May, June, July; ASO: August, September, October; NDJ: November, December, January; FMA: February, March, April.

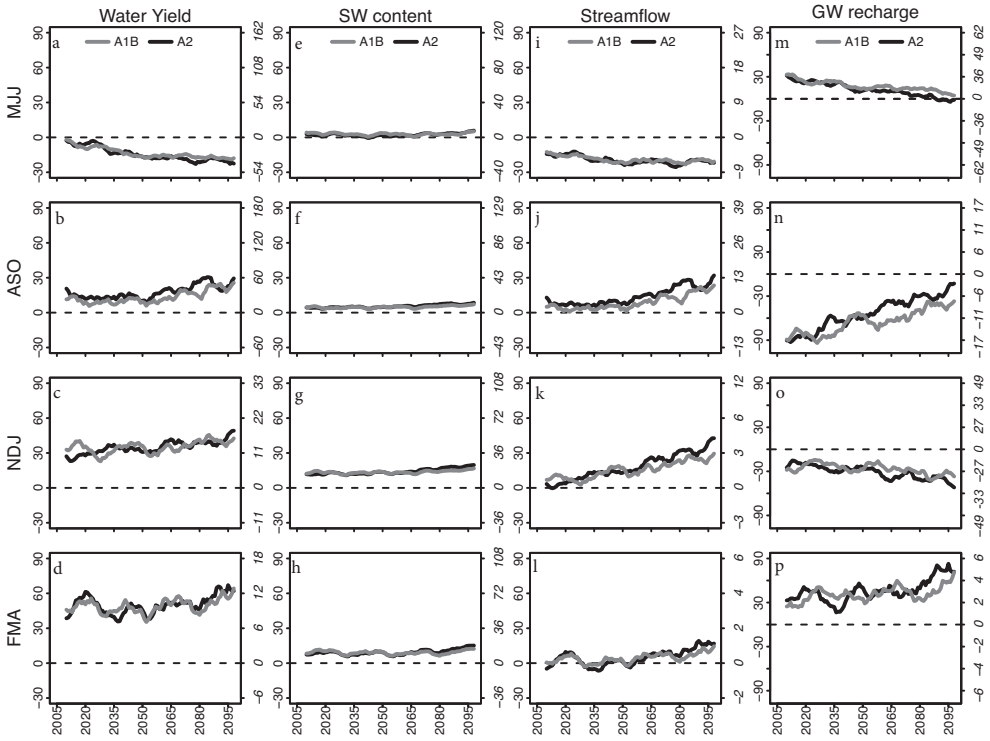

Fig. 7. Projected long-term patterns in total water yield (first column), soil water content (second column), streamflow (third column), and groundwater recharge (fourth column) under the A1B and A2 scenarios simulated in the Soil and Water Assessment Tool from downscaled Canadian Global Coupled Model 3.1 precipitation. The left ordinates show percent change (as deviation from the long-term average). The right ordinates show the simulated values (mm for water yield, soil water content, and groundwater recharge, and thousand $m^3\ s^{-1}$ for the streamflow). The dashed line demarcates the baseline values. MJJ: May, June, July (the early monsoon period); ASO: August, September, October (the later monsoon period); NDJ: November, December, January; and FMA: February, March, April.

predicted with projection range between 27,525 $m^3\ s^{-1}$ and 21,408 $m^3\ s^{-1}$ (10–30% decrease from the baseline) (Fig. 7i) mostly due to predicted decrease in precipitation during the same period. Thereafter, strong increasing trends were detected in the streamflow for the rest of the periods (Table 7). The projected increase in streamflow ranged from 42,547 $m^3\ s^{-1}$ to 55,311 $m^3\ s^{-1}$ (0–30% increase from the baseline) during ASO, and 9912–14,372 $m^3\ s^{-1}$ (0–45% increase from the baseline) during NDJ under A1B and A2 scenarios, respectively (Fig. 7j and k). A sharp increasing period in FMA streamflow was also predicted until 2030 primarily possibly due to increased spring snowmelt. The increasing trend followed thereafter, but with much slower rate in the range between 5455 $m^3\ s^{-1}$ and 6109 $m^3\ s^{-1}$ (0–12% increase from the baseline) (Fig. 7l). The streamflow patterns during FMA suggested that the impacts of spring snowmelt on the streamflow could diminish by 2030. The long-term patterns in the groundwater recharge showed a significant decreasing trend for the early monsoon period (MJJ) and a significant increasing trend for the later monsoon period (ASO) (Fig. 7m–p and Table 7).

5.7. Model uncertainties

Although we analyzed five hydrological components (e.g., total water yield, soil water content, ET, streamflow, and groundwater recharge) simulated in the SWAT model, the model was calibrated and validated using only one component – streamflow. Therefore, predicted estimates of those

components that were not calibrated were more uncertain. However, ET estimates were validated qualitatively with the estimates from the Joint UK Land and Environment Simulator (JULES) model provided by the European Union WATer and Global Change (WATCH) project. Additional uncertainties could also be contributed from (1) uncertainties in the future climate conditions and emission scenarios, (2) errors in GCM predictors, (3) errors in the downscaling of precipitation in SDSM, and (4) errors in the SWAT model. While quantifying many of these uncertainties is often challenging, the interpretation of model results requires consideration of these uncertainties. Analyzing the sources of errors in the projected climate conditions, emission scenarios, and GCM predictor variables was beyond the scope of this study. The uncertainties in the downscaled precipitation used in this study were generated in our earlier work (Pervez and Henebry, 2014). In brief, the bias in the raw CGCM3.1 precipitation was substantially reduced in the downscaled CGCM3.1 precipitation. There were estimated ±29% and ±28% uncertainties in the downscaled CGCM3.1 precipitation for the A1B and A2 scenarios, respectively (Pervez and Henebry, 2014). It is no surprise that these uncertainties associated with downscaled precipitation will propagate to the uncertainty of SWAT-simulated hydrological components. Even though uncertainty in the downscaled precipitation was attenuated, the propagated uncertainty in simulated hydrological components because of the uncertainty in the downscaled precipitation is largely unknown. Furthermore, the projected downscaled precipitation may not be accurate at some future time, because the model developed for the downscaling may not adequately capture the changed environmental conditions in a future climate. As a distributed hydrological model, SWAT is subject to large uncertainties (Rostamian et al., 2008). SUFI2 is one of the uncertainty analysis techniques integrated into SWAT that enables users to quantify model errors more systematically while calibrating the model. We used SUFI2 and discussed the model uncertainties in Sections 3.3 and 5.1.

6. Discussion

The model performance metrics suggested that the SWAT model calibration and validation was satisfactory at the monthly scale, but there were substantial differences between observed and simulated peak streamflow at the daily scale. The high intensity localized precipitation might not have been well represented by the limited number of precipitation stations used in the study. Therefore, the use of a limited number of observed precipitation stations might have contributed to underestimation of extreme events and peak flows at the daily scale. However, as our objective here was to assess long-term impacts rather than impacts from individual events or events over a short time period, the well calibrated and validated model at a monthly scale could be considered acceptable to assess basinwide long-term impacts of climate and land use change (Wu et al., 2012b).

The basinwide total water yield, streamflow, and groundwater recharge were more sensitive to changes in precipitation, while ET and soil water content were more sensitive to changes in physiological forcing and temperature. The impacts of climate and land use change were predicted to be more pronounced for the seasonal variability in hydrological components than the interannual variability, possibly because of the predicted lower interannual variability in the precipitation, and the assumptions of holding historical spatial and temporal distributions of humidity, solar radiation, and wind speed true for the future time. However, sensitivity of the hydrological components to impacts of the changes in humidity, solar radiation, and wind speed were predicted to be minor (Jha et al., 2006).

When nearly all regions of the world were expected to experience a net negative impact of climate change on water resources (Parry, 2007), the climate and land use change impacts outlook on the Brahmaputra basin water resources was predicted to be somewhat positive, although the results of this study indicated the exacerbation of drought and flooding potentials due to predicted decreases in total water yield, soil water content, and streamflow in May–July and a predicted increase in seasonal streamflow and water yield in August–October. An increase in average seasonal streamflow is most likely to increase the number of extreme discharges, because there is a strong relationship between average monthly discharge and maximum monthly discharge (Immerzeel, 2008). The groundwater recharge potentials in the basin were predicted to be higher for the projected climate and land use change scenarios than under current conditions (Fig. 7). However, the prediction estimates did not account for the current and future groundwater withdrawal estimates mostly due to a lack of sufficient regional information on the groundwater withdrawals and future demand projections.

7. Conclusions

The downscaled CGCM3.1 precipitation from CMIP3 and the IMAGE-derived land use corresponding to future climate and land use change scenarios were used to drive the SWAT hydrology model for the Brahmaputra basin. Specific objectives of this study were to assess sensitivity of the basin hydrological responses to changing levels of CO_2 and temperature, and to assess potential impacts of climate and land use change on the freshwater availability in the basin.

The sensitivity scenario results indicated that increase in CO_2 concentration caused basinwide average ET to decrease because of physiological forcing, which resulting in increases in average total water yield, streamflow, and groundwater recharge. The increase in average monthly minimum and maximum temperature caused average ET to increase, and average soil water content and groundwater recharge to decrease. Increase in temperature also caused a decrease in average total water yield and streamflow during the period May through September, but it caused the same to increase during the winter months of January and February. Increase in precipitation resulted in an increase in total water yield, streamflow, and groundwater recharge proportionately but indicated minor effects on ET. The basinwide average ET and soil water content were found more responsive to changes in physiological forcing and temperature, while the total water yield, streamflow, and groundwater recharge were more responsive to changes in precipitation.

The annual average total water yield, soil water content, ET, streamflow, and groundwater recharge were predicted to increase in response to climate and land use change. The impacts of climate and land use change were predicted to be more pronounced for the seasonal variability in hydrological components than the interannual variability in the Brahmaputra basin. The predicted climate and land use change impacts outlook on the Brahmaputra basin water resources was somewhat positive, although the results of the study indicated the exacerbation of flooding potential during August–October, and drought potential during May–July periods of the 21st century. The results presented in this study were based on only one CMIP3 GCM precipitation when multiple CMIP3 and CMIP5 GCM precipitation are available. There is large inter-model variability in the simulation of spatial characteristics of seasonal monsoon precipitation (Sabade et al., 2011); therefore, conclusions based on one downscaled precipitation may not be optimal and may defer when multiple GCMs are considered. However, CMIP5 simulations of Indian summer monsoon rainfall show similar bias and uncertainties over CMIP3 simulations at the original resolution (Shashikanth et al., 2013; Sperber et al., 2013), and the projected global temperature change in CMIP5 is remarkably similar to that from CMIP3 (Knutti and Sedláček, 2013). Therefore, the differences in climate change impacts assessment from CMIP3 and CMIP5 simulation results can be expected to produce similar results.

Our combined analyses of sensitivity of hydrological components to climate change and long-term impacts of future climate and land use change on freshwater availability can offer much needed inputs for resource management and policy decision-making. Given the spatial extent and geophysical and climatic characteristics of the basin, it is more likely that the impacts of climate and land use changes on hydrological components will vary spatially. Therefore, the climate and land use change impacts should also be evaluated at the subbasin level to provide a more complete picture of the potential impacts of projected future climate and land use change on the freshwater availability in the Brahmaputra basin. Yet the availability, as well as the accessibility, of data to support the finer scale analyses may preclude such studies in many areas. However, this study has shown the feasibility of joining land cover and land use change scenarios with climate change projections to produce plausible predictions for multiple hydrological components in a major river basin in a densely populated region of south Asia.

Conflict of interest

None declared.

Acknowledgements

This research was supported in part by the U.S. Agency for International Development Famine Early Warning Systems Network agreement with the U.S. Geological Survey, and in part by the Geospatial

Sciences Center of Excellence at South Dakota State University. We sincerely thank Dr. Gabriel Senay, Dr. James P. Verdin, James Rowland, and Michael Budde at USGS EROS, and Dr. William Capehart at SDSMT for suggestions made throughout the research. We are also thankful to Nancy Sammons at the U.S. Department of Agriculture and Dr. Raghavan Srinivasan at Texas A&M University for guiding in calibration of the model. We greatly appreciate the astute comments made by the anonymous reviewers, and technical comments and edits provided by USGS reviewers that helped us to improve the manuscript. Any use of trade, firm, or product names is for descriptive purposes only and does not imply endorsement by the U.S. Government.

Appendix A.

$$\text{Bias} \quad (\%) = \frac{(1/N)\sum_{i=1}^{N}(X_{\text{sim},i} - X_{\text{obs},i})}{\sum_{i=1}^{N} X_{\text{obs},i}} * 100$$

$$R = \frac{\sum_{i=1}^{N}(X_{\text{obs},i} - \overline{X_{\text{obs}}})(X_{\text{sim},i} - \overline{X_{\text{sim}}})}{\sqrt{\sum_{i=1}^{N}(X_{\text{sim},i} - \overline{X_{\text{sim}}})^2 \sum_{i=1}^{N}(X_{\text{obs},i} - \overline{X_{\text{obs}}})^2}}$$

$$\text{NS} = 1 - \frac{\sum_{i=1}^{N}(X_{\text{sim},i} - X_{\text{obs},i})^2}{\sum_{i=1}^{N}(X_{\text{obs},i} - \overline{X_{\text{obs}}})^2}$$

$$\text{RMSE} = \left[\frac{1}{N}\sum_{i=1}^{N}(X_{\text{sim},i} - X_{\text{obs},i})^2\right]^{1/2}$$

where $X_{\text{obs},i}$ is the ith observed streamflow, $X_{\text{sim},i}$ is the ith simulated streamflow, and N is the number of data records. Percent bias measures the average difference between observations and model simulations. R^2 is the coefficient of determination and describes how much of the residual variance between the observed and simulated variables can be explained through a linear fit. The NS quantitatively describes the accuracy of the model output for the variables, and the RMSE explains the difference between observed and simulated variables.

Appendix B.

See Tables B1 and B2.

Table B1
CO_2 concentration and temperature projections from the Fourth Assessment Report (AR4) of the Intergovernmental Panel on Climate Change (Solomon, 2007).

Run #	Period	CO_2 (ppm)		Temperature (°C)							
		A1B	A2	A1B				A2			
				DJF	MAM	JJA	SON	DJF	MAM	JJA	SON
1	2001–2010	391	390	0.36	0.35	0.27	0.31	0.46	0.45	0.35	0.40
2	2011–2020	420	417	0.72	0.7	0.54	0.62	0.93	0.90	0.69	0.80
3	2021–2030	454	451	1.08	1.05	0.81	0.93	1.39	1.35	1.04	1.20
4	2031–2040	491	490	1.44	1.40	1.08	1.24	1.85	1.80	1.39	1.59
5	2041–2050	532	532	1.80	1.75	1.35	1.55	2.31	2.25	1.74	1.99
6	2051–2060	572	580	2.16	2.10	1.62	1.86	2.78	2.70	2.08	2.39
7	2061–2070	611	635	2.52	2.45	1.89	2.17	3.24	3.15	2.43	2.79
8	2071–2080	649	698	2.88	2.80	2.16	2.48	3.70	3.60	2.78	3.19
9	2081–2090	685	771	3.24	3.15	2.43	2.79	4.17	4.05	3.12	3.59
10	2091–2100	717	856	3.60	3.50	2.70	3.10	4.63	4.50	3.47	3.99
11	2061–2075	611	635	2.52	2.45	1.89	2.17	3.24	3.15	2.43	2.79

Table B2
Downscaled projected changes in land use simulated in Integrated Model to Assess the Global Environment (IMAGE) and future land cover change requirements.

Run	Period	IMAGE projected change in agricultural land									
		A1B					A2				
		Actual IMAGE change (%)	Downscaled change (%)	Downscaled change (m ha)	% of total area	Other LC to agriculture (%)	Actual IMAGE change (%)	Downscaled change (%)	Downscaled change (m ha)	% of total area	Other LC to agriculture (%)
	2000 (USGS, 2000)	–	–	5.6	11.0	–	–	–	5.6	11.0	–
1	2001–2010	17	10	6.2	11.9	3.0	26	18	6.6	12.7	5.5
2	2011–2020	27	17	6.6	12.6	5.0	38	25	7.0	13.5	7.5
3	2021–2030	32	22	6.8	13.2	6.2	60	32	7.4	14.2	9.5
4	2031–2040	59	32	7.4	14.2	9.2	78	50	8.4	16.2	15.0
5	2041–2050	63	36	7.6	14.7	10.3	91	55	8.7	16.7	16.5
6	2051–2060	66	41	7.9	15.2	11.6	128	61	9.0	17.4	18.3
7	2061–2070	75	42	8.0	15.3	11.9	118	71	9.6	18.5	21.3
8	2071–2080	72	41	7.9	15.2	11.6	128	73	9.7	18.7	21.9
9	2081–2090	66	37	7.7	14.8	10.5	134	74	9.8	18.8	22.2
10	2091–2100	65	36	7.6	14.7	10.0	139	76	9.9	19.0	22.8
11	2061–2075	75	42	8.0	15.3	11.9	118	71	9.6	18.5	21.3

References

Abbaspour, K., 2007. User Manual for SWAT-CUP, SWAT Calibration and Uncertainty Analysis Programs. Swiss Federal Institute of Aquatic Science and Technology, Eawag, Duebendorf, Switzerland.

Abbaspour, K., Johnson, C., Van Genuchten, M.T., 2004. Estimating uncertain flow and transport parameters using a sequential uncertainty fitting procedure. Vadose Zone J. 3 (4), 1340–1352.

Abbaspour, K.C., Faramarzi, M., Ghasemi, S.S., Yang, H., 2009. Assessing the impact of climate change on water resources in Iran. Water Resour. Res. 45 (10), W10434.

Alcamo, J., Henrichs, T., 2002. Critical regions: a model-based estimation of world water resources sensitive to global changes. Aquat. Sci. 64 (4), 352–362.

Annamalai, H., Hamilton, K., Sperber, K.R., 2007. The South Asian summer monsoon and its relationship with ENSO in the IPCC AR4 simulations. J. Clim. 20 (6).

Arnell, N.W., 1996. Global Warming, River Flows and Water Resources. John Wiley & Sons Ltd, Chichester, UK.

Arnell, N.W., Liv, C., 2001. Hydrology and water resources. In: McCarthy, J.J., Canziani, O.F., Leary, N.A., Dokken, D.J., White, K.S. (Eds.), Climate Change 2001: Impacts, Adaptation and Vulnerability. Cambridge University Press, Cambridge, pp. 191–233.

Arnold, J.G., Srinivasan, R., Muttiah, R.S., Williams, J.R., 1998. Large area hydrologic modeling and assessment: Part I. Model development. J. Am. Water Resour. Assoc. 34 (1), 73–89.

Ashok, K., Guan, Z., Saji, N.H., Yamagata, T., 2004. Individual and combined influences of ENSO and the Indian Ocean Dipole on the Indian summer monsoon. J. Clim. 17 (16), 3141–3155.

Ashok, K., Saji, N.H., 2007. On the impacts of ENSO and Indian Ocean Dipole events on sub-regional Indian summer monsoon rainfall. Nat. Hazards 42 (2), 273–285.

Baral, P., Kayastha, R.B., Immerzeel, W.W., Pradhananga, N.S., Bharrarai, B.C., Shahi, S., Galos, S., Springer, C., Joshi, S.P., Mool, P.K., 2014. Preliminary results of mass-balance observations of Yala Glacier and analysis of temperature and precipitation gradients in Langtang Valley, Nepal. Ann. Glaciol. 55 (66), 9–14.

Betts, R.A., Boucher, O., Collins, M., Cox, P.M., Falloon, P.D., Gedney, N., Hemming, D.L., Huntingford, C., Jones, C.D., Sexton, D.M.H., Webb, M.J., 2007. Projected increase in continental runoff due to plant responses to increasing carbon dioxide. Nature 448 (7157), 1037–1041.

Betts, R.A., Cox, P.M., Lee, S.E., Woodward, F.I., 1997. Contrasting physiological and structural vegetation feedbacks in climate change simulations. Nature 387, 796–799.

Bookhagen, B., Burbank, D.W., 2006. Topography, relief, and TRMM-derived rainfall variations along the Himalaya. Geophys. Res. Lett. 33 (8).

Brunner, G.W., 2002. HEC-RAS River Analysis System: User's Manual. US Army Corps of Engineers, Institute for Water Resources, Hydrologic Engineering Center.

Cai, W., Zheng, X.-T., Weller, E., Collins, M., Cowan, T., Lengaigne, M., Yu, W., Yamagata, T., 2013. Projected response of the Indian Ocean Dipole to greenhouse warming. Nat. Geosci. 6 (12), 999–1007.

Chu, J.T., Xia, J., Xu, C.Y., Singh, V.P., 2010. Statistical downscaling of daily mean temperature, pan evaporation and precipitation for climate change scenarios in Haihe River, China. Theor. Appl. Climatol. 99 (1–2), 149–161.

Chu, T., Shirmohammadi, A., 2004. Evaluation of the SWAT model's hydrology component in the Piedmont physiographic region of Maryland. Trans. ASAE 47 (4), 1057–1073.

Cibin, R., Sudheer, K., Chaubey, I., 2010. Sensitivity and identifiability of stream flow generation parameters of the SWAT model. Hydrol. Process. 24 (9), 1133–1148.

Cisneros, B.E.J., Oki, T., Arnell, N.W., Benito, G., Cogley, J.G., Döll, P., Jiang, T., Mwakalila, S.S., Fischer, T., Gerten, D., Hock, R., Kanae, S., Lu, X., Mata, L.J., Pahl-Wostl, C., Strzepek, K.M., Su, B., van den Hurk, B., 2014. Climate Change 2014: Impacts, Adaptation, and Vulnerability: Contribution of Working Group II to the Fifth Assessment Report of the Intergovernmental Panel on Climate Change. IPCC.

Costa, M.H., Botta, A., Cardille, J.A., 2003. Effects of large-scale changes in land cover on the discharge of the Tocantins River, Southeastern Amazonia. J. Hydrol. 283 (1), 206–217.

Debele, B., Srinivasan, R., Parlange, J.Y., 2008. Coupling upland watershed and downstream waterbody hydrodynamic and water quality models (SWAT and CE-QUAL-W2) for better water resources management in complex river basins. Environ. Model Assess. 13 (1), 135–153.

Dobrovolski, R., Diniz-Filho, J.A.F., Loyola, R.D., Júnior, P.D.M., 2011. Agricultural expansion and the fate of global conservation priorities. Biodivers. Conserv. 20 (11), 2445–2459.

Environmental Modeling Center, 2010. NCEP Climate Forecast System Reanalysis (CFSR) Monthly Products, January 1979 to December 2010 , Boulder, CO.

FAO, 1995. The Digital Soil Map of the World and Derived Soil Properties. FAO, Rome.

Faramarzi, M., Abbaspour, K.C., Schulin, R., Yang, H., 2009. Modelling blue and green water resources availability in Iran. Hydrol. Process. 23 (3), 486–501.

Ficklin, D.L., Luo, Y., Luedeling, E., Zhang, M., 2009. Climate change sensitivity assessment of a highly agricultural watershed using SWAT. J. Hydrol. 374 (1), 16–29.

Ficklin, D.L., Stewart, I.T., Maurer, E.P., 2013. Climate change impacts on streamflow and subbasin-scale hydrology in the upper Colorado River Basin. PLOS ONE 8 (8), e71297.

Field, C.B., Jackson, R.B., Mooney, H.A., 1995. Stomatal responses to increased CO_2: implications from the plant to the global scale. Plant Cell Environ. 18 (10), 1214–1225.

Fontaine, T.A., Cruickshank, T.S., Arnold, J.G., Hotchkiss, R.H., 2002. Development of a snowfall–snowmelt routine for mountainous terrain for the soil water assessment tool (SWAT). J. Hydrol. 262 (1–4), 209–223.

Gain, A.K., Immerzeel, W.W., Sperna Weiland, F.C., Bierkens, M.F.P., 2011. Impact of climate change on the stream flow of the lower Brahmaputra: trends in high and low flows based on discharge-weighted ensemble modelling. Hydrol. Earth Syst. Sci. 15 (5), 1537–1545.

Gassman, P.W., Reyes, M.R., Green, C.H., Arnold, J.G., 2007. The soil and water assessment tool: historical development, applications, and future research directions. Trans. ASABE 50 (4), 1211–1250.

Gedney, N., Cox, P., Betts, R., Boucher, O., Huntingford, C., Stott, P., 2006. Detection of a direct carbon dioxide effect in continental river runoff records. Nature 439 (7078), 835–838.
Ghaffari, G., Keesstra, S., Ghodousi, J., Ahmadi, H., 2010. SWAT-simulated hydrological impact of land-use change in the Zanjanrood basin, Northwest Iran. Hydrol. Process. 24 (7), 892–903.
Ghosh, S., Dutta, S., 2012. Impact of climate change on flood characteristics in Brahmaputra basin using a macro-scale distributed hydrological model. J. Earth Syst. Sci. 121 (3), 637–657.
Gosain, A., Rao, S., Basuray, D., 2006. Climate change impact assessment on hydrology of Indian river basins. Curr. Sci. 90 (3), 346–353.
Hasson, S., Lucarini, V., Pascale, S., 2013. Hydrological cycle over South and Southeast Asian river basins as simulated by PCMDI/CMIP3 experiments. Earth Syst. Dyn. 4 (2), 199–217.
Havnø, K., Madsen, M., Dørge, J., Singh, V., 1995. MIKE 11 – a generalized river modelling package. Comput. Models Watershed Hydrol., 733–782.
Heuvelmans, G., Muys, B., Feyen, J., 1999. Analysis of the spatial variation in the parameters of the SWAT model with application in Flanders, Northern Belgium. Hydrol. Earth Syst. Sci. 8 (5), 931–939.
Hewitson, B.C., Crane, R.G., 2006. Consensus between GCM climate change projections with empirical downscaling: precipitation downscaling over South Africa. Int. J. Climatol. 26 (10), 1315–1337.
Hijioka, Y., Lin, E., Pereira, J.J., Corlett, R.T., Cui, X., Insarov, G., Lasco, R., Lindgren, E., Surjan, A., Aizen, E.M., Aizen, V.B., Begum, R.A., Baba, K., Chatterjee, M., Cogley, J.G., Diffenbaugh, N., Ding, L., Gao, Q., Garschagen, M., Hashizume, M., Kapshe, M., Kostianoy, A.G., McInnes, K., Nair, S., Prabhakar, S.V.R.K., Saito, Y., Schaffer, A., Shaw, R., Stone, D., Wassman, R., Wilbanks, T.J., Wu, S., 2014. Asia: Climate Change 2014: Impacts, Adaptation, and Vulnerability: Contribution of Working Group II to the Fifth Assessment Report of the Intergovernmental Panel on Climate Change. IPCC.
Houghton, J.T., Ding, Y., Griggs, D.J., Noguer, M., van der Linden, P.J., Dai, X., Maskell, K., Johnson, C., 2001. Climate Change 2001: The Scientific Basis, vol. 881. Cambridge University Press, Cambridge.
Huang, X., Sillanpää, M., Gjessing, E., Peräniemi, S., Vogt, R., 2011. Water quality in the southern Tibetan Plateau: chemical evaluation of the Yarlung Tsangpo (Brahmaputra). River Res. Appl. 27 (1), 113–121.
Hungate, B.A., Reichstein, M., Dijkstra, P., Johnson, D., Hymus, G., Tenhunen, J., Hinkle, C., Drake, B., 2002. Evapotranspiration and soil water content in a scrub-oak woodland under carbon dioxide enrichment. Glob. Change Biol. 8 (3), 289–298.
Huntington, T.G., 2006. Evidence for intensification of the global water cycle: review and synthesis. J. Hydrol. 319 (1), 83–95.
IMAGE Team, 2001. The IMAGE 2.2 Implementation of the SRES Scenarios: A Comprehensive Analysis of Emissions, Climate Change and Impacts in the 21st Century. RIVM CD-ROM Publication, 481508018.
Immerzeel, W.W., 2008. Historical trends and future predictions of climate variability in the Brahmaputra basin. Int. J. Climatol. 28 (2), 243–254.
Immerzeel, W.W., Petersen, L., Ragettli, S., Pellicciotti, F., 2014. The importance of observed gradients of air temperature and precipitation for modeling runoff from a glacierized watershed in the Nepalese Himalayas. Water Resour. Res. 50 (3), 2212–2226.
Immerzeel, W.W., van Beek, L.P.H., Bierkens, M.F.P., 2010. Climate change will affect the Asian water towers. Science 328 (5984), 1382–1385.
Jha, M., Arnold, J.G., Gassman, P.W., Giorgi, F., Gu, R.R., 2006. Climate change sensitivity assessment on Upper Mississippi River Basin streamflows using SWAT. J. Am. Water Resour. Assoc. 42 (4), 997–1016.
Jha, M., Gassman, P.W., Secchi, S.S., Gu, R., Arnold, J.G., 2004a. Effect of watershed subdivision on SWAT flow, sediment, and nutrient predictions. J. Am. Water Resour. Assoc. 40 (3), 811–825.
Jha, M., Pan, Z., Tackle, E.S., Gu, R., 2004b. Impacts of climate change on streamflow in the Upper Mississippi River Basin: a regional climate model perspective. J. Geophys. Res. D: Atmos. 109 (9), D09105 1–12.
Jian, J., Webster, P.J., Hoyos, C.D., 2009. Large-scale controls on Ganges and Brahmaputra River discharge on intraseasonal and seasonal time-scales. Q. J. R. Meteorol. Soc. 135 (639), 353–370.
Jourdain, N.C., Gupta, A.S., Taschetto, A.S., Ummenhofer, C.C., Moise, A.F., Ashok, K., 2013. The Indo-Australian monsoon and its relationship to ENSO and IOD in reanalysis data and the CMIP3/CMIP5 simulations. Clim. Dyn. 41 (11–12), 3073–3102.
Kalnay, E., Kanamitsu, M., Kistler, R., Collins, W., Deaven, D., Gandin, L., Iredell, M., Saha, S., White, G., Woollen, J., Zhu, Y., Chelliah, M., Ebisuzaki, W., Higgins, W., Janowiak, J., Mo, K.C., Ropelewski, C., Wang, J., Leetmaa, A., Reynolds, R., Jenne, R., Joseph, D., 1996. The NCEP/NCAR 40-year reanalysis project. Bull. Am. Meteorol. Soc. 77 (3), 437–471.
Kirsch, K., Kirsch, A., Arnold, J., 2002. Predicting sediment and phosphorus loads in the Rock River basin using SWAT. Forest 971, 10.
Kirtman, B., Power, S.B., Adedoyin, J.A., Boer, G.J., Bojariu, R., Camilloni, I., Doblas-Reyes, F.J., Fiore, A.M., Kimoto, M., Meehl, G.A., Prather, M., Sarr, A., Schär, C., Sutton, R., van Oldenborgh, G.J., Vecchi, G., Wang, H.J., 2013. Near-term climate change: projections and predictability. In: Stocker, T.F., et al. (Eds.), Climate Change 2013: The Physical Science Basis. Contribution of Working Group I to the Fifth Assessment Report of the Intergovernmental Panel on Climate Change. Cambridge University Press, Cambridge, United Kingdom/New York, NY, USA.
Knutti, R., Sedláček, J., 2013. Robustness and uncertainties in the new CMIP5 climate model projections. Nat. Clim. Change 3 (4), 369–373.
Kripalani, R., Oh, J., Kulkarni, A., Sabade, S., Chaudhari, H., 2007. South Asian summer monsoon precipitation variability: coupled climate model simulations and projections under IPCC AR4. Theor. Appl. Climatol. 90 (3–4), 133–159.
Labat, D., Goddéris, Y., Probst, J.L., Guyot, J.L., 2004. Evidence for global runoff increase related to climate warming. Adv. Water Resour. 27 (6), 631–642.
Lehner, B., Döll, P., Alcamo, J., Henrichs, T., Kaspar, F., 2006. Estimating the impact of global change on flood and drought risks in Europe: a continental, integrated analysis. Clim. Change 75 (3), 273–299.
Lehner, B., Verdin, K., Jarvis, A., 2008. New global hydrography derived from spaceborne elevation data. EOS Trans. Am. Geophys. Union 89 (10), 93–94.
Liang, X., Lettenmaier, D.P., Wood, E.F., 1996. One-dimensional statistical dynamic representation of subgrid spatial variability of precipitation in the two-layer variable infiltration capacity model. J. Geophys. Res.: Atmos. (1984–2012) 101 (D16), 21403–21422.

Loveland, T.R., Reed, B.C., Brown, J.F., Ohlen, D.O., Zhu, Z., Yang, L., Merchant, J.W., 2000. Development of a global land cover characteristics database and IGBP DISCover from 1 km AVHRR data. Int. J. Remote Sens. 21 (6–7), 1303–1330.
Luo, Y., He, C., Sophocleous, M., Yin, Z., Hongrui, R., Ouyang, Z., 2008. Assessment of crop growth and soil water modules in SWAT2000 using extensive field experiment data in an irrigation district of the Yellow River Basin. J. Hydrol. 352 (1), 139–156.
Luo, Y., Zhang, M., 2009. Management-oriented sensitivity analysis for pesticide transport in watershed-scale water quality modeling using SWAT. Environ. Pollut. 157 (12), 3370–3378.
Markstrom, S.L., Niswonger, R.G., Regan, R.S., Prudic, D.E., Barlow, P.M., 2008. GSFLOW, Coupled Ground-Water and Surface-Water Flow Model Based on the Integration of the Precipitation-Runoff Modeling System (PRMS) and the Modular Ground-Water Flow Model (MODFLOW-2005). U.S. Department of the Interior, U.S. Geological Survey.
Mirza, M.Q., 2002. Global warming and changes in the probability of occurrence of floods in Bangladesh and implications. Global Environ. Change 12 (2), 127–138.
Montenegro, A., Ragab, R., 2010. Hydrological response of a Brazilian semi-arid catchment to different land use and climate change scenarios: a modelling study. Hydrol. Process. 24 (19), 2705–2723.
Mutenyo, I., Nejadhashemi, P., Woznicki, S., Giri, S., 2013. Evaluation of SWAT performance on a mountainous watershed in tropical Africa. Hydrology: Curr. Res. s14 (001), 1–7.
Nakicenovic, N., Swart, R., 2000. Cambridge University Press, Cambridge, UK.
Nash, J., Sutcliffe, J., 1970. River flow forecasting through conceptual models: Part I. A discussion of principles. J. Hydrol. 10 (3), 282–290.
National Climatic Data Center, 2001. Global Surface Summary of the Day – GSOD, Version 7. National Oceanic and Atmospheric Administration, Ashville, NC.
Oki, T., Kanae, S., 2006. Global hydrological cycles and world water resources. Science 313 (5790), 1068–1072.
Parry, M.L., 2007. Climate Change 2007: Impacts, Adaptation and Vulnerability: Contribution of Working Group II to the Fourth Assessment Report of the Intergovernmental Panel on Climate Change, 4. Cambridge University Press, Cambridge, UK, New York, USA.
Pervez, M.S., Henebry, G.M., 2014. Projections of the Ganges–Brahmaputra precipitation – downscaled from GCM predictors. J. Hydrol. 517, 120–134.
Piao, S., Ciais, P., Huang, Y., Shen, Z., Peng, S., Li, J., Zhou, L., Liu, H., Ma, Y., Ding, Y., 2010. The impacts of climate change on water resources and agriculture in China. Nature 467 (7311), 43–51.
Pomeroy, J., Brun, E., 2001. Physical properties of snow. In: Snow Ecology: An Interdisciplinary Examination of Snow-Covered Ecosystems. Cambridge University Press, Cambridge, UK, pp. 45–126.
Rahman, K., Maringanti, C., Beniston, M., Widmer, F., Abbaspour, K., Lehmann, A., 2013. Streamflow modeling in a highly managed mountainous glacier watershed using SWAT: the Upper Rhone River watershed case in Switzerland. Water Resour. Manage. 27 (2), 323–339.
Rajeevan, M., Bhate, J., Jaswal, A.K., 2008. Analysis of variability and trends of extreme rainfall events over India using 104 years of gridded daily rainfall data. Geophys. Res. Lett. 35 (18), L18707.
Reynolds, C.A., Jackson, T.J., J, R.W., 1999. Estimating available water content by linking the FAO soil map of the world with global soil profile database and pedo-transfer functions. In: AGU 1999 Spring Conference, Boston, MA.
Rossi, C.G., Srinivasan, R., Jirayoot, K., Le Duc, T., Souvannabouth, P., Binh, N., Gassman, P.W., 2009. Hydrologic evaluation of the lower Mekong river basin with the soil and water assessment tool model. Int. Agric. Eng. J. 18 (1–2), 1–13.
Rostamian, R., Jaleh, A., Afyuni, M., Mousavi, S.F., Heidarpour, M., Jalalian, A., Abbaspour, K.C., 2008. Application of a SWAT model for estimating runoff and sediment in two mountainous basins in central Iran. Hydrol. Sci. J. 53 (5), 977–988.
Sabade, S., Kulkarni, A., Kripalani, R., 2011. Projected changes in South Asian summer monsoon by multi-model global warming experiments. Theor. Appl. Climatol. 103 (3–4), 543–565.
Sahin, V., Hall, M.J., 1996. The effects of afforestation and deforestation on water yields. J. Hydrol. 178 (1), 293–309.
Schuol, J., Abbaspour, K.C., Srinivasan, R., Yang, H., 2008. Estimation of freshwater availability in the West African sub-continent using the SWAT hydrologic model. J. Hydrol. 352 (1–2), 30–49.
Sellers, P., Bounoua, L., Collatz, G., Randall, D., Dazlich, D., Los, S., Berry, J., Fung, I., Tucker, C., Field, C., 1996. Comparison of radiative and physiological effects of doubled atmospheric CO_2 on climate. Science 271 (5254), 1402–1406.
Shashikanth, K., Salvi, K., Ghosh, S., Rajendran, K., 2013. Do CMIP5 simulations of Indian summer monsoon rainfall differ from those of CMIP3? Atmos. Sci. Lett. 15 (2), 79–85.
Shi, Y., Gao, X., Zhang, D., Giorgi, F., 2011. Climate change over the Yarlung Zangbo–Brahmaputra River Basin in the 21st century as simulated by a high resolution regional climate model. Quat. Int. 244 (2), 159–168.
Siderius, C., Biemans, H., Wiltshire, A., Rao, S., Franssen, W., Kumar, P., Gosain, A., van Vliet, M., Collins, D., 2013. Snowmelt contributions to discharge of the Ganges. Sci. Total Environ. 468, S93–S101.
Singh, V.P., Sharma, N., Shekhar, C., Ojha, P. (Eds.), 2004. The Brahmaputra Basin Water Resources. Kluwer Academic Publishers, Dordrecht, The Netherlands.
Sleeter, B.M., Sohl, T.L., Bouchard, M.A., Reker, R.R., Soulard, C.E., Acevedo, W., Griffith, G.E., Sleeter, R.R., Auch, R.F., Sayler, K.L., Prisley, S., Zhu, Z., 2012. Scenarios of land use and land cover change in the conterminous United States: utilizing the special report on emission scenarios at ecoregional scales. Global Environ. Change 22 (4), 896–914.
Solomon, S., 2007. Climate Change 2007 – The Physical Science Basis: Working Group I Contribution to the Fourth Assessment Report of the IPCC. Cambridge University Press, Cambridge, UK, New York, USA.
Sperber, K.R., Annamalai, H., Kang, I.-S., Kitoh, A., Moise, A., Turner, A., Wang, B., Zhou, T., 2013. The Asian summer monsoon: an intercomparison of CMIP5 vs. CMIP3 simulations of the late 20th century. Clim. Dyn. 41 (9–10), 2711–2744.
Srinivasan, R., Arnold, J.G., Jones, C.A., 1998a. Hydrologic modelling of the United States with the Soil and Water Assessment Tool. Int. J. Water Resour. Dev. 14 (3), 315–325.
Srinivasan, R., Ramanarayanan, T.S., Arnold, J.G., Bednarz, S.T., 1998b. Large area hydrologic modeling and assessment: Part II. Model application. J. Am. Water Resour. Assoc. 34 (1), 91–101.

Stockle, C.O., Williams, J.R., Rosenberg, N.J., Jones, C.A., 1992. A method for estimating the direct and climatic effects of rising atmospheric carbon dioxide on growth and yield of crops: Part I. Modification of the EPIC model for climate change analysis. Agric. Syst. 38 (3), 225–238.
Sun, C., Ren, L., 2013. Assessment of surface water resources and evapotranspiration in the Haihe River basin of China using SWAT model. Hydrol. Process. 27 (8), 1200–1222.
Thayyen, R.J., Gergan, T.J., Dobhal, D.P., 2005. Slope lapse rates of temperature in Din Gad (Dokriani Glacier) catchment, Garhwal Himalaya, India. Bull. Glaciol. Res. 22, 31–37.
Tibebe, D., Bewket, W., 2011. Surface runoff and soil erosion estimation using the SWAT model in the Keleta watershed, Ethiopia. Land Degrad. Dev. 22 (6), 551–564.
Tiwari, V., Wahr, J., Swenson, S., 2009. Dwindling groundwater resources in northern India, from satellite gravity observations. Geophys. Res. Lett. 36 (18).
Tolson, B.A., Shoemaker, C.A., 2004. Watershed Modeling of the Cannonsville Basin Using SWAT2000: Model. Cornell University, Ithaca, NY.
Ullrich, A., Volk, M., 2009. Application of the Soil and Water Assessment Tool (SWAT) to predict the impact of alternative management practices on water quality and quantity. Agric. Water Manage. 96 (8), 1207–1217.
van Griensven, A., Meixner, T., Grunwald, S., Bishop, T., Diluzio, M., Srinivasan, R., 2006. A global sensitivity analysis tool for the parameters of multi-variable catchment models. J. Hydrol. 324 (1), 10–23.
Vörösmarty, C.J., Green, P., Salisbury, J., Lammers, R.B., 2000. Global water resources: vulnerability from climate change and population growth. Science 289 (5477), 284–288.
Webster, P.J., Jian, J., 2011. Environmental prediction, risk assessment and extreme events: adaptation strategies for the developing world. Philos. Trans. R. Soc. A: Math. Phys. Eng. Sci. 369 (1956), 4768–4797.
Wetterhall, F., Bárdossy, A., Chen, D., Halldin, S., Xu, C.Y., 2009. Statistical downscaling of daily precipitation over Sweden using GCM output. Theor. Appl. Climatol. 96 (1–2), 95–103.
Wilby, R.L., Dawson, C.W., Barrow, E.M., 2002. SDSM – a decision support tool for the assessment of regional climate change impacts. Environ. Model. Softw. 17 (2), 147–159.
Wilby, R.L., Hay, L.E., Leavesley, G.H., 1999. A comparison of downscaled and raw GCM output: implications for climate change scenarios in the San Juan River Basin, Colorado. J. Hydrol. 225 (1–2), 67–91.
Winchell, M., Srinivasan, R., Di Luzio, M., Arnold, J., 2010. ArcSWAT Interface for SWAT 2009. USDA Agricultural Research Service and Texas A&M Blackland Research Center, Temple, Texas.
Wu, Y., Liu, S., Abdul-Aziz, O.I., 2012a. Hydrological effects of the increased CO_2 and climate change in the Upper Mississippi River Basin using a modified SWAT. Clim. Change 110 (3–4), 977–1003.
Wu, Y., Liu, S., Gallant, A.L., 2012b. Predicting impacts of increased CO_2 and climate change on the water cycle and water quality in the semiarid James River Basin of the Midwestern USA. Sci. Total Environ. 430, 150–160.